J. Fluid Mech. (2001), *vol.* 444, *pp.* 343–382. Printed in the United Kingdom

Reynolds-number dependence of turbulent velocity and pressure increments

By B. R. PEARSON AND R. A. ANTONIA

Department of Mechanical Engineering, University of Newcastle, NSW, 2308, Australia

(Received 29 March 1999 and in revised form 20 April 2001)

The main focus is the Reynolds number dependence of Kolmogorov normalized low-order moments of longitudinal and transverse velocity increments. The velocity increments are obtained in a large number of flows and over a wide range (40–4250) of the Taylor microscale Reynolds number R_λ. The R_λ dependence is examined for values of the separation, r, in the dissipative range, inertial range and in excess of the integral length scale. In each range, the Kolmogorov-normalized moments of longitudinal and transverse velocity increments increase with R_λ. The scaling exponents of both longitudinal and transverse velocity increments increase with R_λ, the increase being more significant for the latter than the former. As R_λ increases, the inequality between scaling exponents of longitudinal and transverse velocity increments diminishes, reflecting a reduced influence from the large-scale anisotropy or the mean shear on inertial range scales. At sufficiently large R_λ, inertial range exponents for the second-order moment of the pressure increment follow more closely those for the fourth-order moments of transverse velocity increments than the fourth-order moments of longitudinal velocity increments. Comparison with DNS data indicates that the magnitude and R_λ dependence of the mean square pressure gradient, based on the joint-Gaussian approximation, is incorrect. The validity of this approximation improves as r increases; when r exceeds the integral length scale, the R_λ dependence of the second-order pressure structure functions is in reasonable agreement with the result originally given by Batchelor (1951).

1. Introduction

The first two similarity hypotheses of Kolmogorov (1941, hereinafter referred to as K41) provided a simple description of the small-scale structure of turbulence within the framework of local isotropy and very large Reynolds numbers. According to the first hypothesis, moments of the longitudinal velocity increment $\delta u \equiv u(x+r) - u(x)$ depend only on $\langle\epsilon\rangle$, the mean energy dissipation rate (the angular brackets denote time averaging) and the kinematic viscosity ν of the fluid, when the separation r is sufficiently small, i.e. within the viscous-dissipative range (DR). When r is in the inertial range (IR), the effect of ν can be neglected and $\langle(\delta u)^n\rangle \sim r^{n/3}$. A third hypothesis – the refined similarity hypothesis – (RSH) was introduced by Kolmogorov (1962) to account for the spatial intermittency of the dissipative field.

One consequence of RSH is that the IR power-law exponents of r need no longer be given by $n/3$; in general, $\langle(\delta u)^n\rangle \sim r^{\zeta_u(n)}$, where $\zeta_u(n) \neq n/3$. Significant attention has been given through models, experiments and numerical simulations (Kolmogorov 1962; She & Leveque 1994; Anselmet *et al.* 1984; Arneodo *et al.* 1996; Cao, Chen & She 1996) to the dependence of $\zeta_u(n)$ on either n or R_λ. The similarity

hypotheses do not distinguish between moments of longitudinal velocity increments or transverse velocity increments. Recently, experiments (Herweijer & Van de Water 1995; Kahalerras, Malecot & Gagne 1996; Noullez *et al.* 1997) and simulations (Chen *et al.* 1997) have shown that the scaling exponents associated with transverse increments may be slightly smaller than longitudinal increments. Other experiments have show them to be significantly smaller (Antonia & Pearson 1997) especially for shear flows at low to moderate R_λ. Some of these differences can be explained by the lack of a common measurement of the transverse increment and or a common definition of its relative scaling exponent.

There is evidence (Arneodo *et al.* 1996) to suggest that $\zeta_u(n)$ does not change appreciably with R_λ in shear-free flows. There is also partial evidence (Camussi & Benzi 1997; Chen *et al.* 1997; Dhruva, Tsuji & Sreenivasan 1997; Zhou & Antonia 2000) to indicate that the magnitudes of $\zeta_v(n)$ or $\zeta_w(n)$, where v and w are transverse velocity fluctuations, may increase with R_λ, leaving open the possibility that at asymptotically large R_λ, $\zeta_u(n)$, $\zeta_v(n)$ and $\zeta_w(n)$ will all be equal. Another consequence of RSH is that moments of velocity derivatives, normalized by Kolmogorov variables, can now depend on R_λ instead of remaining constant (K41). In particular, the overwhelming majority of the available data indicate that the magnitude of the flatness factor $F_{\partial u/\partial x} \equiv \langle(\partial u/\partial x)^4\rangle/\langle(\partial u/\partial x)^2\rangle^2$ of $\partial u/\partial x$ increases monotonically with R_λ (see the compilations of Van Atta & Antonia 1980 and Sreenivasan & Antonia 1997). An exception to this trend is the measurements of Tabeling *et al.* (1996) in a flow of helium gas at 5° K contained between two counter-rotating disks. The magnitude of $F_{\partial u/\partial x}$ increases with R_λ up to $R_\lambda \simeq 700$ before decreasing for $R_\lambda > 700$. Tabeling *et al.* speculate that the 'transitional' behaviour around $R_\lambda \simeq 700$ may be associated with the instability and breakdown of intense vortex filaments (Jimenez *et al.* 1993). While Sreenivasan & Antonia (1997) noted that there were several unresolved problems with respect to Tabeling *et al.*'s experiment, an interesting feature of that experiment was the ability to cover a significant range of R_λ in the same flow. For one of the flows (plane jet) that we consider, R_λ was varied from about 500 to about 1400, thus straddling the transitional Reynolds number of the Tabeling *et al.* experiment. The possibility of the 'transitional' behaviour being flow dependent cannot of course be ruled out. There is less information available for the dependence of $F_{\partial v/\partial x}$ on R_λ; the limited data (Antonia, Zhou & Shafi 1996) to date suggest that for $R_\lambda \leqslant 200$, $F_{\partial v/\partial x}$ increases with R_λ at a rate comparable to that for $F_{\partial u/\partial x}$. The wake data of Antonia *et al.* (1996) indicate that the magnitude of $F_{\partial v/\partial x}$ is larger than that of $F_{\partial u/\partial x}$ but comparable to that of either $F_{\partial u/\partial y}$ or F_{ω_z}, where ω_z is the spanwise vorticity fluctuation; the significant difference between $F_{\partial u/\partial y}$ and $F_{\partial u/\partial x}$ is also evident in numerical simulations (Jimenez *et al.* 1993). Perhaps consistently with the previous observations, several authors (Kahalerras *et al.* 1996; Chen *et al.* 1997) suggested that δv should be associated with enstrophy whereas δu is more probably linked to ϵ. This suggestion was made primarily to explain the difference between $\zeta_u(n)$ and $\zeta_v(n)$, the scaling exponents for $\langle(\delta u)^n\rangle$ and $\langle(\delta v)^n\rangle$, in the IR.

The present paper focuses mainly on the R_λ dependence of the low-order moments of δu^* and δv^*, the asterisk denoting normalization by Kolmogorov length [$\eta \equiv (\nu^3/\langle\epsilon\rangle)^{1/4}$] or velocity ($u_K \equiv \nu/\eta$) scales. In particular, the emphasis is on the R_λ behaviour of these structure functions for three different ranges of the separation r, namely

(i) the dissipative range DR with r^* typically less than 20,
(ii) the inertial range IR ($1 \ll r^* \ll L^*$),
(iii) and when r^* exceeds the integral lengthscale L^*.

We are not aware of any other investigation where the Reynolds-number dependence in all three ranges has been considered for data that cover a wide R_λ range (about 40–4250) and are treated in a consistent manner (see § 2). The interest in (i) is partly to investigate whether Kolmogorov-normalized moments of δu and δv exhibit a Reynolds-number dependence. We also consider the R_λ dependencies of the skewness $S_{\partial u/\partial x} \equiv \langle(\partial u/\partial x)^3\rangle/\langle(\partial u/\partial x)^2\rangle^{3/2}$ and $F_{\partial u/\partial x}$ and whether $\langle(\partial v^*/\partial x^*)^4\rangle$ or $\langle(\partial u^*/\partial x^*)^2(\partial v^*/\partial x^*)^2\rangle$ varies with R_λ in a different manner from $\langle(\partial u^*/\partial x^*)^4\rangle$. The interest in $\langle(\partial u^*/\partial x^*)^2(\partial v^*/\partial x^*)^2\rangle$ stems from its inclusion in the formulation of $\langle(\delta p^*)^2\rangle$ (the second-order pressure structure function) by Hill & Wilczak (1995). With respect to (ii), the emphasis is primarily on the difference in the magnitudes of exponents associated with δu and δv and whether this difference disappears as R_λ increases. The behaviour of range (iii) is important in terms of establishing the R_λ dependence of moments of either velocity or pressure in the context of likely departures from global isotropy and Gaussianity of the velocity field.

We also consider the R_λ dependence of $\langle(\delta p^*)^2\rangle$ (p is the kinematic pressure fluctuation), a quantity closely linked to fourth-order velocity increment moments. The earliest investigations into the behaviour of $\langle(\delta p^*)^2\rangle$ or, equivalently, the two-point pressure correlation were based on the assumption of the joint-Gaussianity approximation (JGA), applied either in the form used by Millionshchikov (1941) or in terms of the independence of Fourier components of velocity (Heisenberg 1948). JGA has been used here to calculate $\langle(\delta p^*)^2\rangle$ from the measured distributions of $\langle(\delta u^*)^2\rangle$. The R_λ dependence of $\langle(\delta p^*)^2\rangle$ is then examined for the three ranges mentioned above. In particular, we estimate the R_λ dependencies of $\langle p^{*2}\rangle$, scaling range exponents of $\langle(\delta p^*)^2\rangle$ and the mean-square pressure gradient $\langle(\partial p^*/\partial x^*)^2\rangle$. Since JGA is unlikely to be accurate at small values of r^* (Kim & Antonia 1993; Hill 1994), the accuracy of $\langle(\partial p^*/\partial x^*)^2\rangle$ has been assessed by comparison with results obtained from direct numerical simulations and with the use of a relation (Hill & Wilczak 1995) which avoids JGA.

Experimental details, including the procedure used for treating the data, are given in § 2. Low-order moments of δu and δv are considered in § 3 whereas third-order moments are discussed in § 4. The data for second-order moments of δp are treated in § 5. Although § 3, § 4 and § 5 address the R_λ dependence of separations ranging from dissipative to integral scales, we deal with the R_λ dependence of IR exponents, corresponding to moments of both velocity and pressure increments, in § 6. A discussion of the possible effect of anisotropy on these exponents is included in § 6.

2. Experimental conditions

2.1. *Introduction and flow conditions*

A significant amount of two velocity component data from a number of different flows over a wide range of R_λ [$\equiv u'\lambda/\nu$, $\lambda = u'/\langle(\partial u/\partial x)^2\rangle^{1/2}$, $40 \lesssim R_\lambda \lesssim 4250$) (the maximum R_λ available for only u component data was about 5630) was analysed for this paper. Strictly, a definition of R_λ based on u' and λ is ambiguous in non-isotropic turbulence (e.g. Corrsin 1963; Fulachier & Antonia 1983). However, while the use of the fluctuating vector u_i should result in a more general definition of the turbulence Reynolds number, the velocity fluctuations u, v and w were measured in only a few flows; for convenience, the present and generally used definition of R_λ has been retained. The majority of data were acquired for the current study. Some of the other data were obtained in our laboratory and were used in previously reported

investigations; they were re-analysed for the present paper. The remaining data were acquired and published by other researchers. The following flows were used:

(*a*) Grid turbulence $R_\lambda \sim 68$ (Antonia, Zhou & Zhu 1998*b*) cf. table 1.

(*b*) Cylinder wakes $R_\lambda \sim 38, 39$ (Antonia & Pearson 1998) and $R_\lambda \sim 210$ (Antonia & Pearson 1997) cf. table 1.

(*c*) Rough wall boundary layer $R_\lambda \sim 330$ (Antonia & Smalley 2000) cf. table 1.

(*d*) Circular jet $R_\lambda \sim 500$ (current study) cf. table 1.

(*e*) Pipe (current study) – single-wire ($67 \lesssim R_\lambda \lesssim 337$) cf. table 2; X-wire data ($68 \lesssim R_\lambda \lesssim 335$) cf. table 3.

(*f*) Plane jets – single-wire ($500 \lesssim R_\lambda \lesssim 1400$, current study; Pearson & Antonia 1997) cf. tables 4(*a*) and 4(*b*); X-wire data $R_\lambda \sim 535$ (Antonia *et al.* 1997*a*), $666 \lesssim R_\lambda \lesssim 1170$ (current study) cf. table 5.

(*g*) atmospheric surface layers $R_\lambda \sim 5630$ (Zhu, Antonia & Hosokawa 1995), $R_\lambda \sim 4250$ (current study) $R_\lambda \sim 10\,340$–$14\,860$ (Dhruva *et al.* 1997; their table II) and $R_\lambda \sim 19\,500$ (Sreenivasan & Dhruva 1998; their figures 3, 4 and 5) cf. table 1.

In each flow, a crossed hot-wire probe was used to measure u and v (or w) velocity fluctuations. Pertinent experimental conditions are summarized in tables 1–5. Investigations of flows (*a*) to (*f*) were carried out in our laboratory; the experimental facilities for (*a*), (*b*), (*c*) and parts of (*f*) and (*g*) have been described elsewhere. The data for the circular and plane jets are new, as are the pipe flow data; a brief description of these facilities will be given below. The atmospheric surface layer data, designated 'current study' in (*g*), were acquired by a group, which included the second author, at the 1976 International Turbulence Comparison Experiment (ITCE) – although the experiments by this group were not part of the main ITCE program (Dyer *et al.* 1982). These data had not been previously analysed in terms of small-scale statistics. A brief description of the experimental set-up will also be given below.

For the circular jet (*d*), two component measurements are made on the centreline with a X-wire probe. The Reynolds number ($Re = U_j d/\nu$, where U_j is the jet exit velocity and D is the 55 mm diameter of the jet nozzle) is 170 000. Measurements are made at $x/D \simeq 60$ where the flow field should be self-preserving (Antonia, Satyaprakash & Hussain 1980). Only one value of R_λ (~ 500) has been measured. Each wire, of diameter 2.54 μm (Pt-10% Rh), is etched to a length of 0.5 mm ($l^* = 3.3$); the Kolmogorov normalized transverse separation between wires is 2.2. The X-probe is calibrated for velocity and yaw at the jet exit plane. Further details can be found in table 1; acquisition and calibration details are further discussed below.

The pipe used for (*e*) is high-grade drawn aluminium of internal diameter $D \equiv 127$ mm. The complete length is 18.96 m (149 diameters). Air is drawn into the pipe, via a fibreglass moulded bellmouth, and immediate transition-to-turbulence is ensured with a high-grit sandpaper roughness strip (1 diameter width). Single and two-component velocity measurements are made. The probe (either the single- or X-wire) is located a distance of $100D$ downstream of the trip. Pressure taps are located along the complete pipe length and the measured mean static pressure gradient, for each value of U_1 (centreline velocity), is constant beyond the initial development length region. The linearity of the pressure and the measured high-order moments of u and v on the pipe centreline indicated that the assumption of fully developed flow is satisfactory at the measurement station. The yaw calibration is carried out *in situ* with special care to ensure the probe is maintained at the centreline for each angle. A Pitot-static tube, for calibration purposes, is located a further sixteen diameters downstream. The single wire is 1.27 μm Pt-10% Rh with an etched length of 0.25 mm. The Kolmogorov-normalized wire length was in the range $0.8 \leqslant l^* \leqslant 3.6$

https://doi.org/10.1017/S0022112001005511 Published online by Cambridge University Press

Flow type	$\frac{y}{\delta}$	R_λ	$\langle U\rangle$ ($\frac{\mathrm{m}}{\mathrm{s}}$)	u' ($\frac{\mathrm{m}}{\mathrm{s}}$)	v' ($\frac{\mathrm{m}}{\mathrm{s}}$)	$\langle\epsilon\rangle^a$ ($\frac{\mathrm{m}^2}{\mathrm{s}^3}$)	$\langle\epsilon\rangle^b$ ($\frac{\mathrm{m}^2}{\mathrm{s}^3}$)	$\pm 95\%$ ($\frac{\mathrm{m}^2}{\mathrm{s}^3}$)	η (mm)	U_k ($\frac{\mathrm{m}}{\mathrm{s}}$)	f_s (Hz)	f_k (Hz)	f_c/f_κ	L_u (m)	L_v (m)	N	T_s (s)
Grid	—	68	11.3	0.22	0.18	0.53	0.45	0.05	0.292	0.052	12 600	6157	1.02	0.046	0.010	74 377	610
C-W1a	0.0	38	3.25	0.09	0.08	0.044	0.039	0.00	0.543	0.028	1667	954	0.84	0.046	0.010	31 807	895
C-W1b	0.0	39	3.27	0.09	0.07	0.046	0.042	0.00	0.535	0.029	1667	972	0.82	0.046	0.007	31 807	895
C-W2a	0.0	195	12.6	0.82	—	12.5	11.0	1.02	0.133	0.116	25 000	15 107	0.83	0.130	—	3176	66
C-W2b	0.0	201	12.4	0.82	0.77	12.0	9.6	0.69	0.136	0.113	27 027	14 541	0.93	0.098	0.013	5191	82
C-W2c	0.0	205	12.4	0.82	0.78	12.0	9.6	1.00	0.136	0.113	27027	14 517	0.93	0.101	0.026	5043	82
RWBL	0.5	330	14.3	2.13	1.60	207.0	153.0	37.1	0.068	0.230	50 000	33 622	0.74	0.034	0.009	71 136	336
C-J	—	485	4.31	1.12	0.94	6.90	6.46	0.97	0.149	0.100	8000	4616	0.87	0.166	0.071	13 609	1049
ASLa	$5m$	5630	3.25	0.79	—	0.0123	—	0.0006	0.778	0.019	1333	715	0.88	—	—	—	692
ASLb	$2m$	4250	6.2	0.94	0.43	0.041		0.006	0.535	0.028	10 000	1844	0.68	84.1	9.72	62	1678
ABLa																	
ABLb																	

Grid, Antonia *et al.* (1998*b*).
C-W1a, cylinder wake $u-v$; C-W1b, cylinder wake $u-w$; current study.
C-W2a, cylinder wake u; C-W2b, cylinder wake $u-v$; C-W2c, cylinder wake $u-w$; Antonia *et al.* (1996).
RWBL, rough wall boundary layer; Antonia & Smalley (2000).
C-J, circular jet; current study.
ASLa, atmospheric surface layer; Zhu *et al.* (1995).
ASLb, atmospheric surface layer; current study.
ABLa, atmospheric boundary layer; Dhruva *et al.* (1997); see their table I for details (35 m above ground level; $R_\lambda \approx 10\,000 - 15\,000$).
ABLb, atmospheric boundary layer; Sreenivasan & Dhruva (1998); see their table I Run 3 for details ($R_\lambda \approx 19\,500$).
δ, is the boundary layer thickness or wake/jet half-width; y, is the distance from the wall or from the wake/jet centreline.
[a] $\langle\epsilon\rangle \approx 15\nu\langle(\partial u/\partial x)^2\rangle$; $\langle(\partial u/\partial x)^2\rangle$ is calculated from the structure function method using $\langle(\partial u/\partial x)^2\rangle \equiv \lim_{r\to 0}\langle(\delta u)^2/r^2\rangle$.
[b] $\langle\epsilon\rangle \approx 15\nu\langle(\partial u/\partial x)^2\rangle$; $\langle(\partial u/\partial x)^2\rangle$ is calculated from the spectral method using $\langle(\partial u/\partial x)^2\rangle \equiv \int_0^\infty k_1^2\phi_u(k_1)\mathrm{d}k_1$.
L_u, longitudinal integral lengthscale $\equiv \langle U\rangle\int_0^{\tau_0}\rho_{uu}(\tau)\mathrm{d}\tau$, $\rho_{uu}(\tau)$ is the longitudinal autocorrelation function and τ_0 is the time at the first zero crossing.
L_v, transverse integral lengthscale $\equiv \langle U\rangle\int_0^{\tau_0}\rho_{vv}(\tau)\mathrm{d}\tau$, $\rho_{vv}(\tau)$ is the transverse autocorrelation function.
N, number of independent samples $\equiv \langle U\rangle T_s/2L_u$.
T_s, total record time.

TABLE 1. Miscellaneous single and X-wire measurement details.

https://doi.org/10.1017/S0022112001005511 Published online by Cambridge University Press

y/R	R_λ	$\langle U\rangle$ ($\frac{\mathrm{m}}{\mathrm{s}}$)	u' ($\frac{\mathrm{m}}{\mathrm{s}}$)	$\langle\epsilon\rangle^a$ ($\frac{\mathrm{m}^2}{\mathrm{s}^3}$)	$\langle\epsilon\rangle^b$ ($\frac{\mathrm{m}^2}{\mathrm{s}^3}$)	$\pm 95\%$ ($\frac{\mathrm{m}^2}{\mathrm{s}^3}$)	η (mm)	U_k ($\frac{\mathrm{m}}{\mathrm{s}}$)	f_s (Hz)	f_k (Hz)	f_c/f_k	L_u (m)	N	T_s (s)	S^*
1.0	65	5.35	0.19	0.277	0.323	0.05	0.333	0.046	5000	2560	0.98	0.033	68 439	839	0.00
1.0	75	5.47	0.20	0.264	0.321	0.04	0.341	0.046	5000	2553	0.98	0.033	17 312	210	0.00
1.0	85	7.58	0.27	0.668	0.668	0.05	0.277	0.057	8000	4352	0.92	0.065	30 514	524	0.00
1.0	98	8.80	0.32	1.035	1.035	0.10	0.248	0.064	10 000	5637	0.89	0.052	35 638	419	0.00
1.0	99	9.05	0.33	1.074	1.274	0.17	0.237	0.065	12 659	6085	1.04	0.048	30 776	331	0.00
0.7	100	5.21	0.25	0.367	0.445	0.06	0.309	0.050	5000	2688	0.93	0.054	40 804	839	0.09
1.0	117	12.29	0.44	2.62	2.62	0.30	0.197	0.080	20 000	9925	1.01	0.056	46 013	419	0.00
0.5	127	4.91	0.32	0.585	0.717	0.09	0.274	0.056	5000	2851	0.88	0.065	31 486	839	0.12
1.0	129	15.26	0.54	4.36	5.72	1.14	0.164	0.094	25 000	14 773	0.85	0.047	54 354	336	0.00
1.0	151	17.27	0.62	6.13	6.13	1.00	0.159	0.099	33 333	17 247	0.93	0.057	38 230	252	0.00
0.7	147	8.63	0.44	1.47	1.77	0.21	0.218	0.071	12 659	6292	1.00	0.082	17 475	331	0.08
0.8	160	15.17	0.61	4.63	5.67	0.89	0.164	0.094	25 000	14 764	0.85	0.058	44 272	336	0.04
1.0	174	21.02	0.74	9.93	9.93	1.50	0.143	0.110	33 333	23 360	0.68	0.057	46 223	252	0.00
1.0	169	23.31	0.86	17.7	19.5	2.66	0.119	0.130	66 667	31 297	1.01	0.044	33 404	126	0.00
0.5	177	8.05	0.54	2.40	2.85	0.33	0.194	0.080	12 659	6625	0.95	0.097	13 797	331	0.10
0.7	186	14.85	0.70	6.38	7.17	1.13	0.153	0.101	25 000	15 481	0.81	0.069	36 383	336	0.06
0.8	197	23.21	0.93	18.4	19.6	2.46	0.118	0.131	66 667	31 303	1.01	0.048	30 367	126	0.03
0.5	230	14.09	0.86	9.02	11.2	1.74	0.138	0.112	25 000	16 231	0.77	0.074	31 768	336	0.08
0.7	245	25.96	1.20	28.2	35.3	5.60	0.113	0.142	50 000	36 451	0.69	0.048	90 363	336	0.05
0.6	278	25.37	1.34	35.0	42.8	3.45	0.107	0.150	50 000	37 826	0.66	0.054	78 789	336	0.07
0.5	311	24.93	1.49	42.3	53.3	8.77	0.096	0.166	50 000	41 171	0.61	0.058	72 519	336	0.07
0.4	333	24.31	1.63	52.1	66.7	11.6	0.092	0.176	50 000	42 386	0.59	0.058	70 437	336	0.07

[a] $\langle\epsilon\rangle \approx 15\nu\langle(\partial u/\partial x)^2\rangle$; $\langle(\partial u/\partial x)^2\rangle$ is calculated from the spectral method using $\langle(\partial u/\partial x)^2\rangle \equiv \int_0^\infty k_1^2\phi_u(k_1)\,\mathrm{d}k_1$.

[b] $\langle\epsilon\rangle \approx 15\nu\langle(\partial u/\partial x)^2\rangle$; $\langle(\partial u/\partial x)^2\rangle$ is calculated from the structure function method using $\langle(\partial u/\partial x)^2\rangle \equiv \lim_{r\to 0}\langle(\delta u)^2/r^2\rangle$.

S^* non-dimensional mean-shear $\equiv (\nu/\langle\epsilon\rangle)^{1/2}\partial\langle U\rangle/\partial y$.

TABLE 2. Pipe single wire measurement details (current study).

https://doi.org/10.1017/S0022112001005511 Published online by Cambridge University Press

y/R	R_λ	$\langle U\rangle$ ($\frac{\mathrm{m}}{\mathrm{s}}$)	u' ($\frac{\mathrm{m}}{\mathrm{s}}$)	v' ($\frac{\mathrm{m}}{\mathrm{s}}$)	$\langle\epsilon\rangle^a$ ($\frac{\mathrm{m}^2}{\mathrm{s}^3}$)	$\langle\epsilon\rangle^b$ ($\frac{\mathrm{m}^2}{\mathrm{s}^3}$)	$\pm 95\%$ ($\frac{\mathrm{m}^2}{\mathrm{s}^3}$)	η (mm)	U_k ($\frac{\mathrm{m}}{\mathrm{s}}$)	f_s (Hz)	f_k (Hz)	f_c/f_k	L_u (m)	L_v (m)	N	T_s (s)	S^*
1.0	62	6.51	0.201	0.170	0.372	0.458	0.07	0.308	0.050	6349	3366	0.94	0.038	0.008	56 737	661	0.00
1.0	64	5.40	0.195	0.170	0.298	0.379	0.05	0.324	0.048	5000	2655	0.94	0.035	0.008	64 564	839	0.00
0.8	71	5.37	0.208	0.173	0.324	0.396	0.03	0.319	0.049	5000	2677	0.93	0.053	0.008	42 833	839	0.06
0.8	78	6.54	0.231	0.192	0.462	0.444	0.02	0.301	0.051	6349	3456	0.91	0.048	0.008	45 008	660	0.06
1.0	85	8.77	0.335	0.282	1.495	1.872	0.20	0.218	0.072	10 000	6410	0.78	0.051	0.008	71 874	839	0.00
0.7	91	6.50	0.278	0.218	0.632	0.753	0.08	0.271	0.057	6349	3820	0.82	0.056	0.008	38 284	661	0.09
1.0	104	8.90	0.355	0.296	1.356	1.510	0.13	0.225	0.069	10 000	6303	0.79	0.047	0.008	39 949	419	0.00
1.0	111	11.32	0.427	0.332	2.521	2.782	0.16	0.193	0.080	16 000	9351	0.86	0.053	0.008	56 212	524	0.00
1.0	135	15.35	0.578	0.443	5.625	6.402	0.68	0.157	0.098	25 000	15 552	0.80	0.060	0.008	43 135	336	0.00
1.0	136	20.15	0.715	0.568	12.62	14.86	1.27	0.128	0.121	50 000	25 098	1.00	0.051	0.008	33 020	168	0.00
1.0	144	25.67	0.943	0.752	35.36	38.77	5.50	0.100	0.155	50 000	40 942	0.61	0.042	0.008	50 777	168	0.00
1.0	163	26.36	0.924	0.742	24.2	27.9	6.22	0.111	0.142	33 333	37 845	0.42	0.044	0.008	74 707	252	0.00
0.7	259	26.03	1.256	0.866	30.01	40.04	9.42	0.103	0.153	33 333	40 285	0.40	0.071	0.009	46 275	252	0.06
0.5	304	24.44	1.490	0.934	43.81	59.06	4.15	0.093	0.169	33 333	41 696	0.38	0.083	0.008	37 092	252	0.08
0.3	326	23.73	1.760	1.053	70.95	100.2	27.08	0.082	0.192	33 333	46 022	0.35	0.083	0.011	35 990	252	0.08

[a] $\langle\epsilon\rangle \approx 15\nu\langle(\partial u/\partial x)^2\rangle$; $\langle(\partial u/\partial x)^2\rangle$ is calculated from the spectral method using $\langle(\partial u/\partial x)^2\rangle \equiv \int_0^\infty k_1^2\phi_u(k_1)\,\mathrm{d}k_1$.

[b] $\langle\epsilon\rangle \approx 15\nu\langle(\partial u/\partial x)^2\rangle$; $\langle(\partial u/\partial x)^2\rangle$ is calculated from the structure function method using $\langle(\partial u/\partial x)^2\rangle \equiv \lim_{r\to 0}\langle(\delta u)^2/r^2\rangle$.

TABLE 3. Pipe X-wire measurement details (current study).

https://doi.org/10.1017/S0022112001005511 Published online by Cambridge University Press

R_λ	$\langle U\rangle$ ($\frac{\mathrm{m}}{\mathrm{s}}$)	u' ($\frac{\mathrm{m}}{\mathrm{s}}$)	$\langle\epsilon\rangle^a$ ($\frac{\mathrm{m}^2}{\mathrm{s}^3}$)	$\langle\epsilon\rangle^b$ ($\frac{\mathrm{m}^2}{\mathrm{s}^3}$)	$\pm 95\%$ ($\frac{\mathrm{m}^2}{\mathrm{s}^3}$)	η (mm)	U_k ($\frac{\mathrm{m}}{\mathrm{s}}$)	f_s (Hz)	f_k (Hz)	f_c/f_k	L_u (m)	N	T_s (s)
498	2.56	0.77	1.31	1.60	0.17	0.218	0.068	3205	1876	0.86	0.290	11 824	2682
569	2.91	0.83	1.29	1.70	0.23	0.214	0.068	5000	2165	1.15	0.376	406	105
580	4.53	1.06	3.46	4.18	0.53	0.170	0.087	6329	4252	0.74	0.275	14 550	1766
696	4.90	1.23	4.25	5.09	0.40	0.165	0.092	12 658	4740	1.33	0.272	991	110
770	5.76	1.43	6.43	8.07	0.90	0.143	0.101	10 000	6390	0.78	0.308	10 444	1117
771	8.92	2.16	32.8	39.8	3.87	0.099	0.153	25 000	14 413	0.87	0.213	2334	111
763	2.08	0.54	0.126	0.158	0.02	0.396	0.038	1613	836	0.96	0.452	14 616	6346
811	4.01	1.23	3.147	3.93	0.46	0.173	0.085	8000	3692	1.08	0.389	1563	303
831	4.00	1.11	2.07	2.40	0.18	0.194	0.076	7042	3278	0.96	0.381	1586	302
851	8.02	1.99	20.42	24.15	3.01	0.108	0.134	16 129	11 788	0.68	0.282	9933	698
867	3.77	0.95	0.987	1.146	0.10	0.239	0.063	4762	2513	0.92	0.430	4820	1101
923	5.83	1.81	11.57	14.03	1.46	0.125	0.117	16 129	7417	1.08	0.423	896	130
940	4.59	1.46	4.732	5.74	0.56	0.157	0.094	10 000	4654	1.07	0.394	1754	301
970	9.04	2.12	19.03	23.45	3.11	0.113	0.134	16 129	12 744	0.63	0.267	2923	173
998	3.81	1.02	0.909	1.226	0.21	0.239	0.063	5000	2540	0.98	0.421	1244	1049
1036	5.14	1.66	6.59	7.76	0.62	0.145	0.101	12 658	5641	1.12	0.420	1836	300
1075	5.76	1.86	9.23	11.4	1.04	0.132	0.111	16 129	6921	1.16	0.431	2007	301
1091	7.62	2.34	23.5	27.8	2.74	0.105	0.139	25 000	11 538	1.08	0.403	992	105
1109	13.81	3.28	83.45	102.4	8.79	0.078	0.193	50 000	28 203	0.89	0.247	778	28
1121	5.81	1.98	11.24	13.55	1.17	0.126	0.116	20 000	7317	1.37	0.412	2126	301
1105	11.73	2.97	61.57	70.67	9.81	0.083	0.176	33 333	22 608	0.71	0.255	5788	252
1133	12.93	3.11	71.38	78.7	11.4	0.080	0.182	33 333	25 751	0.62	0.249	8702	335
1180	8.96	2.69	36.07	41.53	3.13	0.095	0.154	33 333	15 042	1.06	0.398	1173	104
1145	14.38	4.08	208.7	201.1	16.7	0.065	0.238	33 333	34 973	0.46	0.295	16 351	671
1257	10.62	3.16	59.2	69.9	6.03	0.083	0.176	50 000	20 244	1.23	0.381	1452	104
1274	11.00	3.47	83.4	99.8	9.78	0.076	0.191	50 000	22 886	1.09	0.379	1512	104
1336	14.54	4.21	170.9	169.5	17.6	0.068	0.226	33 333	33 933	0.47	0.287	33 933	1174
1371	13.60	3.99	139.4	123.7	6.10	0.073	0.212	25 000	29 817	0.42	0.291	10 442	447

[a] $\langle\epsilon\rangle \approx 15\nu\langle(\partial u/\partial x)^2\rangle$; $\langle(\partial u/\partial x)^2\rangle$ is calculated from the spectral method using $\langle(\partial u/\partial x)^2\rangle \equiv \int_0^\infty k_1^2\phi_u(k_1)\,\mathrm{d}k_1$.

[b] $\langle\epsilon\rangle \approx 15\nu\langle(\partial u/\partial x)^2\rangle$; $\langle(\partial u/\partial x)^2\rangle$ is calculated from the structure function method using $\langle(\partial u/\partial x)^2\rangle \equiv \lim_{r\to 0}\langle(\delta u)^2/r^2\rangle$.

These data are attenuated; for the better part 16-bit resolution should have been used.

TABLE 4. Plane jet single wire measurement details (current study).

https://doi.org/10.1017/S0022112001005511 Published online by Cambridge University Press

R_λ	$\langle U\rangle$ ($\frac{\mathrm{m}}{\mathrm{s}}$)	u' ($\frac{\mathrm{m}}{\mathrm{s}}$)	v' ($\frac{\mathrm{m}}{\mathrm{s}}$)	$\langle\epsilon\rangle^a$ ($\frac{\mathrm{m}^2}{\mathrm{s}^3}$)	$\langle\epsilon\rangle^b$ ($\frac{\mathrm{m}^2}{\mathrm{s}^3}$)	$\pm 95\%$ ($\frac{\mathrm{m}^2}{\mathrm{s}^3}$)	η (mm)	U_k ($\frac{\mathrm{m}}{\mathrm{s}}$)	f_s (Hz)	f_k (Hz)	f_c/f_k	L_u (m)	L_v (m)	N	T_s (s)
506	8.72	2.07	1.88	73.5	71.2	9.19	0.082	0.181	25 000	16 825	0.74	0.093	0.062	2306	49
662	5.81	1.27	1.13	5.31	6.25	0.75	0.160	0.097	8000	5780	0.69	0.226	0.116	13 463	1049
731	4.96	1.25	1.05	4.15	4.82	0.69	0.167	0.091	6329	4719	0.67	0.303	0.118	14 427	1775
764	5.64	1.34	1.16	4.85	5.78	0.74	0.163	0.095	6300	5498	0.57	0.255	0.129	7320	666
789	8.40	1.83	1.60	16.2	18.4	1.54	0.122	0.128	16 129	11 006	0.73	0.226	0.112	9660	524
1107	14.86	3.22	2.84	83.1	85.0	9.60	0.082	0.191	33 333	28 732	0.56	0.240	0.126	7790	252
1077	16.69	3.71	3.34	176.63	136.2	40.0	0.071	0.223	33 333	37 626	0.43	0.216	0.119	9729	252

[a] $\langle\epsilon\rangle \approx 15\nu\langle(\partial u/\partial x)^2\rangle$; $\langle(\partial u/\partial x)^2\rangle$ is calculated from the spectral method using $\langle(\partial u/\partial x)^2\rangle \equiv \int_0^\infty k_1^2\phi_u(k_1)\,\mathrm{d}k_1$.

[b] $\langle\epsilon\rangle \approx 15\nu\langle(\partial u/\partial x)^2\rangle$; $\langle(\partial u/\partial x)^2\rangle$ is calculated from the structure function method using $\langle(\partial u/\partial x)^2\rangle \equiv \lim_{r\to 0}\langle(\delta u)^2/r^2\rangle$.

These data are attenuated; for the better part 16-bit resolution should have been used.

TABLE 5. Plane jet X-wire measurement details (current study).

for $67 \lesssim R_\lambda \lesssim 337$. The X-wires are 2.5 μm Pt-10% Rh, with an etched length (l^*) range of 1.2–4.6 and wire separation of approximately 1.8η–4.5η depending on R_λ ($62 \lesssim R_\lambda \lesssim 335$). The Reynolds number ($U_1 D/\nu$; U_1 is the mean velocity on the pipe axis) range investigated is 50 000–220 000 and the majority of measurements are made on the axis; those that are not have non-zero mean-shear, S^*, $[\equiv (\nu/\langle\epsilon\rangle)^{1/2}\partial\langle U\rangle/\partial y]$ and are indicated in tables 2 and 3.

Two different blower-type wind tunnels and nozzle geometries are used for generating the plane jet flows (f). Both tunnels are supplied by variable frequency controlled centrifugal-type blowers. The more extensive single- and X-wire measurements are made downstream of a horizontal two-dimensional nozzle (two-dimensional contraction ratio of 10, width $h = 165$ mm) located at a height of 1.2 m above the floor. A few X-wire measurements were made in a jet exiting from a vertical two-dimensional contraction (ratio = 14) with $h = 42$ mm with the lower edge only 100 mm above the floor. For $h = 165$ mm, u and v is measured at $x = 50h$ from the nozzle exit plane. At this location, the flow is expected to be approximately self-preserving. The jet exit velocity, U_j, could be varied in the range 5 m s^{-1} to 40 m s^{-1}. R_λ, at the measurement station, was in the range 500–1400. The single wire (1.27 μm diameter Pt-10% Rh Wollaston, etched length $l = 0.25$ mm, $0.9 \leqslant l^* \leqslant 3.8$) measurements were made first; a few results were presented and discussed in Pearson & Antonia (1997). The X-wire measurements (2.54 μm, $l \simeq 0.38$ mm, $2.3 \leqslant l^* \leqslant 5.2$ – we had difficulty maintaining a 1.27 μm X-wire probe in this flow) are made over a smaller and less extensive R_λ range (666–1175) than the single wire experiment. A previous simultaneous u and v measurement (Antonia *et al.* 1997*a*) is included here. The measurements were made on the centreline at $53h$ from the exit plane of the 42 mm nozzle with an X-probe (2.5 μm diameter wire of 0.5 mm length). U_j was 25 m s^{-1} and R_λ was 600 (adjusted in this paper to 535) at the measurement station.

Velocity and temperature fluctuations were measured during ITCE 1976. The experiment was conducted on a flat open grazing terrain 15 km NNW of Conargo, near Deniliquin, NSW, Australia. The site was moderately covered by salt bush and native grasses of about 0.5 m in height and there were patches of eucalypt trees, 5–15 m in height, about 5 km SW of the site, in the prevailing wind direction. All velocity, temperature and some cup anemometer signals were recorded on a 4-channel 3960 Hewlett–Packard FM tape recorder. A small selection of X-wire measurements, e.g. horizontal and vertical velocity components, u and v, have been digitized for the current study. The X-wire probe was located at 1.7 m height and consists of two 5 μm diameter Wollaston wires (Pt-10% Rh) of approximately 1 mm etched length in a 90° 'X' configuration. Pertinent flow conditions include $\langle U\rangle \sim 6.2$ m s^{-1}, $\langle u^2\rangle^{1/2} \sim 0.94$ m s^{-1}, $R_\lambda \sim 4250$ and $\eta \sim 0.54$ mm for $z/L \sim -0.03$ (z is the height and L is the Monin–Obukhov lengthscale). For this experiment, the wires were operated by DISA 55M01 constant temperature bridges and signals were conditioned before tape recording. Average bridge output voltages were noted approximately every 2 min and up to 40 min records were obtained. The calibrations, using King's law, of each X-wire were rechecked in the laboratory after returning to Newcastle.

2.2. *Data acquisition and reduction methods*

For all the velocity calibrations, whether single or X-wire probe, velocity versus d.c. voltage curves were obtained both before and after data acquisition. Third- or fourth-order velocity-voltage polynomials were sufficient to describe the wire behaviour. All X-wire measurements were reduced to u and v components using the effective angle method of Browne, Antonia & Chua (1989).

Data were acquired with in-house constant temperature anemometers at an overheat ratio of 1.5. Signal conditioning was achieved with an in-house amplifier/low-pass filter (24 dB/octave) combination. The signal was buck-and-gained to fill at least 70% of the available 10 V range. In most cases, the low-pass cut-off frequency – we avoid aliasing for all of our experimental data sets in this paper by sampling, at least, at twice the low-pass filter frequency – was set to a frequency that was slightly lower than that indicative of the onset of f^2 anemometer noise using a trial-and-error method, i.e. a small sample was acquired and the digital spectrum was calculated on the data acquisition PC. The choice of this *ad hoc* method was justified, especially for the high R_λ flows which have a power spectrum greater than 72 dB (i.e. 12-bit resolution). The resulting voltage signal was digitized with 12-bit resolution. In nearly all cases, the total record length time was limited to 15 min.

For all of our laboratory data, the velocity increments, derivatives and spectra are measured in the time domain. We make use of Taylor's hypothesis to convert from the time to the spatial domain. Most of the data, e.g. (*c*)–(*g*), have high values of $u'/\langle U\rangle$, and should be corrected in the high-wavenumber/small-scale range. We have not applied any corrections – except for the technique discussed in the next subsection – since the majority of this paper deals with scales outside the DR. In tables 1–5 we estimated the number of independent samples, $N \equiv T_s/2T_u$ (Tennekes & Lumley 1972) and consider it to be indicative of the worst-case scenario. Here, T_s is the total record length time and T_u is the integral time scale ($\equiv \int_0^{\tau_0} \rho_{uu}(\tau)\,\mathrm{d}\tau$; where $\rho_{uu}(\tau)$ is the longitudinal velocity autocorrelation function and τ_0 is the time at which the first zero crossing occurs).

2.3. *The estimation of* $\langle\epsilon\rangle$

In this paper, the mean turbulent energy dissipation rate or just $\langle\epsilon\rangle_{iso}$ is calculated by two methods which should be consistent, depending on the degree of homogeneity of the flow. The first method uses the longitudinal one-dimensional spectrum, $\phi_u(k_1)$, namely $\langle\epsilon\rangle = 15\nu\int_0^\infty k_1^2\phi_u(k_1)\,\mathrm{d}k_1$. The compensated spectrum is corrected at high wavenumber by removing the portion of the measured spectrum that deviates from the first-order exponential assumption $\phi_u(k_1) \sim k_1^{-5/3}\exp(mk_1 + b)$ where m and b are constants. The corrected compensated spectrum is then extrapolated. Wherever possible, a sub-record length of approximately $16L_u$ is used. The second method – its level of correspondence to the first depends on the degree of homogeneity of the flow – uses $\langle(\delta u)^2\rangle$ to estimate $\langle(\partial u/\partial x)^2\rangle$, namely $\langle\epsilon\rangle \sim \lim_{r\to 0} 15\nu\langle(\delta u)^2\rangle/r^2$. Here, to remain consistent with the first method, the band of separations corresponding to the high-wavenumber part of the spectrum that deviated from the exponential extrapolation used in the first method is also ignored. A crude approximation is used to convert the frequencies that correspond to the single and double arrows in figure 1 to the required nth time lag, i.e. $\tau_n \sim f_s/f_n$, f_s is the sampling frequency and f_n is the frequency that corresponds to the single or double arrow (the actual conversion is, most probably, more complicated, i.e. dependent on the degree of local homogeneity, at least, and the validity of Taylor's hypothesis). A cubic spline is fitted between these two r scales. The resulting cubic splines are used as weighting functions to extrapolate high-order polynomials to $r = 0$. The resulting value for $\langle\epsilon\rangle$ and its final uncertainty can be found in tables 1–5. The greater inequality when spectra are used, again, may indicate a lack of local-homogeneity or failure of Taylor's hypothesis at high wavenumber/small scales. Higher-order derivatives, e.g. $\langle(\partial u/\partial x)^4\rangle$, $\langle(\partial v/\partial x)^4\rangle$ and $\langle(\partial u/\partial x)^2(\partial v/\partial x)^2\rangle$, are also corrected in this manner. Figure 1 shows an example for the fourth-order moments for the same plane jet data as used in the above

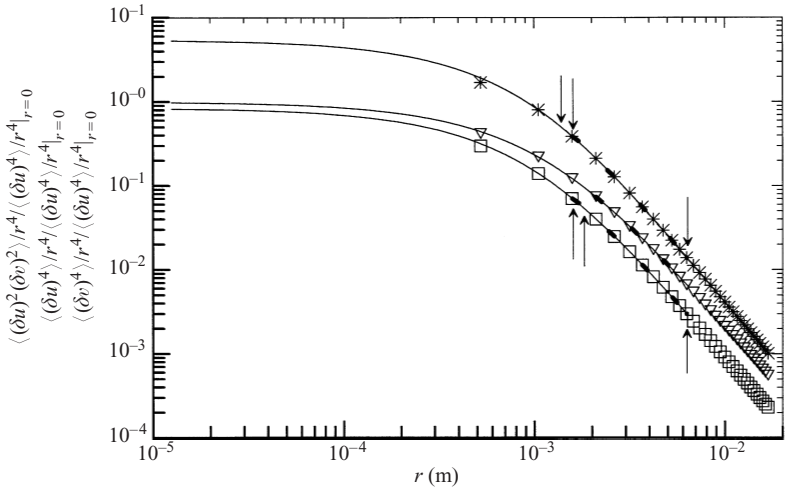

FIGURE 1. r^{-4} compensated fourth-order moments of δu and δv in terms of r. Each curve is 'post'-normalized by the resulting $\langle(\delta u)^2\rangle_{r=0}$. ∇, $\langle(\delta u)^4\rangle$; $*$, $\langle(\delta v)^4\rangle$; $\square$, $\langle(\delta u)^2(\delta v)^2\rangle$; – – –, spline fit to δu or δv or $\delta u\delta v$; —, 'averaged' extrapolation to $r = 0$. $\uparrow$ and $\uparrow\uparrow$ indicate the start and finish of the extrapolation weighting region, as described in the text.

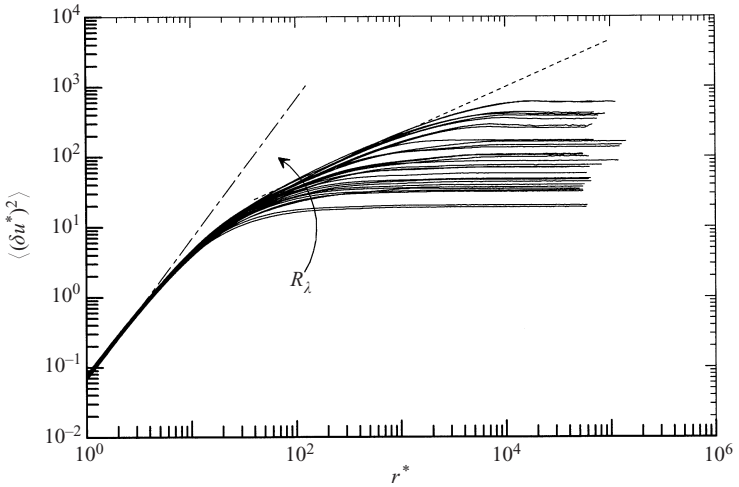

FIGURE 2. A comparison between Kolmogorov-normalized second-order moments of δu (in terms of r^* for $R_\lambda \sim 40 - 1175$) and K41 asymptotes. The arrow points to the direction of increasing R_λ. The increase in the IR slope is evident with R_λ. The data for figures 3–8 are X-wire measurements only (tables 1, 3 and 5). —, $\langle(\delta u^*)^2\rangle$; — - —, $(\frac{1}{15})r^{*2}$; - - -, $\simeq 2.13r^{*2/3}$.

discussion for $\langle\epsilon\rangle$. The results have been normalized by $\langle(\partial u/\partial x)^4\rangle|_{r=0}$. We realize that this technique is empirical; indeed, we have applied (Antonia, Pearson & Zhu 2000) higher-order versions of Batchelor's parameterization method (e.g. Stolovitzky, Sreenivasan & Juneja 1993) on a number of datasets and achieved little improvement in the overall uncertainty for the above quantities at small r^*.

3. Low-order moments of velocity increments

In this section, we discuss low even-order moments of δu^* and δv^*, mainly up to order 6. The discussion on $\langle(\delta u^*)^3\rangle$ will be given in § 4. Second-order moments of

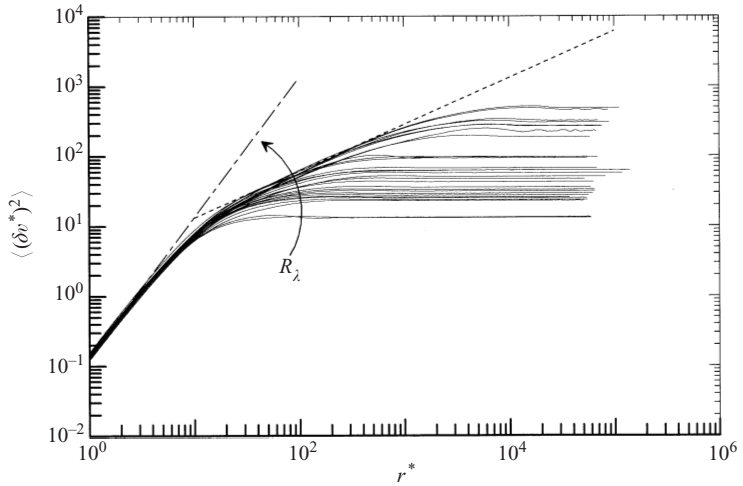

FIGURE 3. Kolmogorov-normalized second-order moments of δv in terms of r^*. Refer to figure 2. —, $\langle(\delta v^*)^2\rangle$; — - —, $(\frac{2}{15})r^{*2}$; - - -, $\simeq (4/3 \times 2.1)r^{*2/3}$.

the velocity increments δu^* and δv^* are plotted in figures 2 and 3 in terms of r^*. As has been reported previously, though only in the context of $\langle(\delta u^*)^2\rangle$ (Anselmet *et al.* 1984; Arneodo *et al.* 1996), the distributions tend to collapse as $r^* \to 0$. This collapse is biased in the case of $\langle(\delta u^*)^2\rangle$ since isotropy was assumed to estimate $\langle\epsilon\rangle$, namely $\langle\epsilon\rangle_{iso} = 15\nu\langle(\partial u/\partial x)^2\rangle$, and $r^{-2}\langle(\delta u)^2\rangle$ was one of two constraints, as discussed in §2. For values of r^* in the DR, the distributions begin to fan out in a systematic fashion as R_λ increases. The smaller R_λ, the smaller the r^* location at which peeling off occurs. The peel-off rate for $\langle(\delta v^*)^2\rangle$ is slightly faster than $\langle(\delta u^*)^2\rangle$ at any given r^*, e.g. for $r^* = 10$ the spread in $\langle(\delta v^*)^2\rangle$ is 1.4 and the spread in $\langle(\delta u^*)^2\rangle$ is 1.2; for $r^* = 50$ the spread in $\langle(\delta v^*)^2\rangle$ is 2.1 and the spread in $\langle(\delta u^*)^2\rangle$ is 2.0. At large r^*, typically greater than L^*, the distributions must attain constant values since $\langle(\delta u^*)^2\rangle \to 2\langle u^*\rangle^2$ and $\langle(\delta v^*)^2\rangle \to 2\langle v^*\rangle^2$ if the flows are decorrelated and homogeneous. All the distributions in figures 2 and 3 seem to conform with this behaviour. The overall behaviour of the distributions in figures 2 and 3 implies that K41 may be approached asymptotically, i.e. similarity of Kolmogorov-normalized distributions is likely to be attained only as $R_\lambda \to \infty$, i.e. fully developed turbulence for which Kolmogorov (1941) and Kolmogorov (1962) were intended.

Distributions of $\langle(\delta u^*)^4\rangle$ and $\langle(\delta v^*)^4\rangle$ are shown in figures 4 and 5, respectively. The general features exhibited by these distributions are similar to those in figures 2 and 3. As expected, the dependence on R_λ appears to be more emphasized for the higher-order moments for figures 4 and 5 than in figures 2 and 3. The increase when $r^* \to 0$ is obvious and non-negligible for both $\langle(\delta u^*)^4\rangle$ and $\langle(\delta v^*)^4\rangle$. For $r^* \simeq 10$, the magnitude of $\langle(\delta u^*)^4\rangle$ increases by a factor of 2.7 while $\langle(\delta v^*)^4\rangle$ increases by about a factor of 3.5 for the R_λ range considered. For $r^* \simeq 50$, the magnitude of $\langle(\delta u^*)^4\rangle$ increases by a factor of 4.1 while $\langle(\delta v^*)^4\rangle$ increases by about a factor of 7.6. In fact, up to $r^* \simeq 200$, the rate of increase in $\langle(\delta v^*)^4\rangle$ appears to be twice that of $\langle(\delta u^*)^4\rangle$ (e.g. 11.1 and 26.3, respectively). In general, the higher rate of increase in $\langle(\delta v^*)^n\rangle$ over that of $\langle(\delta u^*)^n\rangle$ is not surprising, considering that if in the asymptote both must be equal, then $\langle(\delta v^*)^n\rangle$ must increase at a higher rate to catch up to $\langle(\delta u^*)^n\rangle$.

We first examine the R_λ dependence of $\langle(\delta u^*)^{2n}\rangle$ and $\langle(\delta v^*)^{2n}\rangle$, for $n = 1, 2$ and 3, in the asymptotic limit $r^* \to \infty$ (here, $r^* \gg L^*$). It is relatively easy to show,

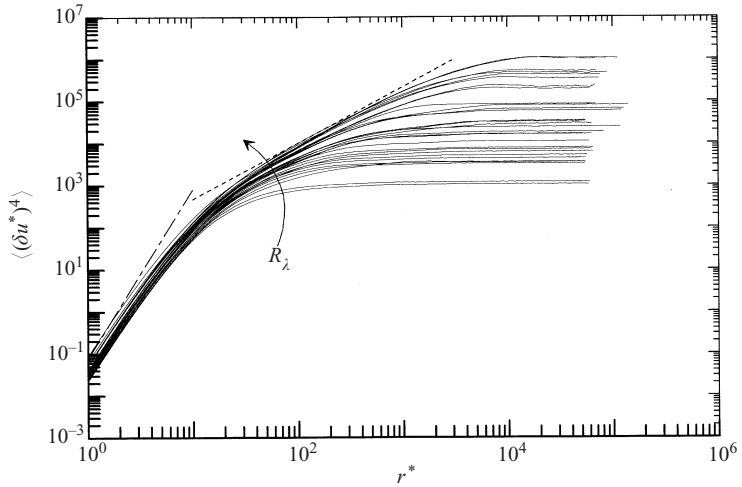

FIGURE 4. Kolmogorov-normalized fourth-order moments of δu in terms of r^*. Refer to figure 2. — - —, $0.07r^{*4}$; - - -, $21.5r^{*4/3}$.

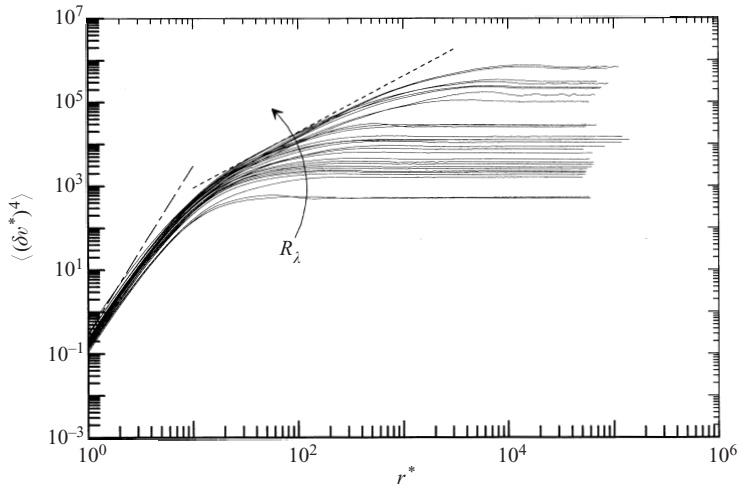

FIGURE 5. Kolmogorov-normalized fourth-order moments of δv in terms of r^*. Refer to figure 3. — - —, $0.3r^{*4}$; - - -, $41.8r^{*4/3}$.

assuming independence of variables and homogeneity, that the limiting values of the second-order quantities are given, using local isotropy, by

$$\langle(\delta u^*)^2\rangle_{r^*\to\infty} = 2\langle u^{*2}\rangle = \frac{2R_\lambda}{\sqrt{15}}, \tag{3.1}$$

$$\langle(\delta v^*)^2\rangle_{r^*\to\infty} = 2\langle v^{*2}\rangle = \frac{2\alpha_{uv}R_\lambda}{\sqrt{15}}, \tag{3.2}$$

where $\alpha_{uv} = \langle v^2\rangle/\langle u^2\rangle$, the ratio of the velocity variances, is considered here to be an indicator of the anisotropy at large scales. The limiting values of $\langle(\delta u^*)^4\rangle$ and $\langle(\delta v^*)^4\rangle$ may be written

$$\langle(\delta u^*)^4\rangle_{r^*\to\infty} = 2\langle u^{*4}\rangle + 6\langle u^{*2}\rangle^2 = 2[F_u + 3]\langle u^{*2}\rangle^2 = 2[F_u + 3]R_\lambda^2/15, \tag{3.3}$$

$$\langle(\delta v^*)^4\rangle_{r^*\to\infty} = 2\langle v^{*4}\rangle + 6\langle v^{*2}\rangle^2 = 2[F_v + 3]\langle v^{*2}\rangle^2 = 2\alpha_{uv}^2[\beta F_u + 3]R_\lambda^2/15, \tag{3.4}$$

where F_u and F_v are the flatness factors [$\equiv \langle a^4\rangle/\langle a^2\rangle^2$, $a = u$ or v] of u and v, respectively, and $\beta = F_v/F_u$. We can easily extend our discussion to the $2n$th-order moment, but experimentally we will suffer errors due to non-closure of the δu and δv p.d.f.s. For $n = 3$,

$$\begin{aligned}\langle(\delta u^*)^6\rangle_{r^*\to\infty} &= 2\langle u^{*6}\rangle + 30\langle u^{*4}\rangle\langle u^{*2}\rangle = 2[SF_u + 15F_u]\langle u^{*2}\rangle^3 \\ &= 2[SF_u + F_u]R_\lambda^3/15^{3/2},\end{aligned} \tag{3.5}$$

$$\begin{aligned}\langle(\delta v^*)^6\rangle_{r^*\to\infty} &= 2\langle v^{*6}\rangle + 30\langle v^{*4}\rangle\langle\ v^{*2}\rangle = 2[SF_v + 15F_v]\langle v^{*2}\rangle^3 \\ &= 2\alpha_{uv}^3[\delta SF_u + \beta F_u]R_\lambda^3/15^{3/2},\end{aligned} \tag{3.6}$$

and SF_u and SF_v are the super flatness factors [$\equiv \langle a^6\rangle/\langle a^2\rangle^3, a = u$ or v] of u and v and $\delta = SF_v/SF_u$. It is worth noting that whilst both β and δ are $\simeq 1$, α_{uv} is, for most flows, smaller than 1 and increasingly contributes to relations (3.2), (3.4) and (3.6) to the power $\frac{1}{2}n$. This suggests that the large-scale quantity α_{uv} could be a considerable contributor to the IR scaling inequality (to be discussed in § 6.3).

We can simplify (3.3)–(3.6) by assuming that the p.d.f.s of u and v are Gaussian, i.e. $F_u = F_v = 3$ and $SF_u = SF_v = 15$

$$\langle(\delta u^*)^4\rangle_{r^*\to\infty} = \tfrac{4}{5}R_\lambda^2 = 3\langle(\delta u^*)^2\rangle_{r^*\to\infty}^2, \tag{3.7}$$

$$\langle(\delta v^*)^4\rangle_{r^*\to\infty} = \tfrac{4}{5}\alpha_{uv}^2R_\lambda^2 = 3\langle(\delta v^*)^2\rangle_{r^*\to\infty}^2. \tag{3.8}$$

Similarly, it is easy to show that

$$\langle(\delta u^*)^2(\delta v^*)^2\rangle_{r^*\to\infty} = 4\langle(u^{*2})(v^{*2})\rangle \simeq 4\alpha_{uv}\langle u^{*2}\rangle^2 \equiv \tfrac{4}{15}\alpha_{uv}R_\lambda^2, \tag{3.9}$$

$$\langle(\delta u^*)^6\rangle_{r^*\to\infty} = \frac{120}{15^{3/2}}R_\lambda^3 = 15\langle(\delta u^*)^2\rangle_{r^*\to\infty}^3, \tag{3.10}$$

$$\langle(\delta v^*)^6\rangle_{r^*\to\infty} = \frac{120}{15^{3/2}}\alpha_{uv}^3R_\lambda^2 = 15\langle(\delta v^*)^2\rangle_{r^*\to\infty}^3. \tag{3.11}$$

These alternative expressions for the limiting values of $\langle(\delta u^*)^4\rangle$, $\langle(\delta v^*)^4\rangle$, $\langle(\delta u^*)^6\rangle$ and $\langle(\delta v^*)^6\rangle$ may also have been obtained by assuming that, for large r^*, the p.d.f.s of δu^* and δv^* are Gaussian. Note that no such assumption is required for $\langle(\delta u^*)^2(\delta v^*)^2\rangle_{r^*\to\infty}$. Equations (3.7)–(3.11) show that the assumption of a Gaussian velocity results in a Gaussian structure function. In practice, the p.d.f.s of u and v are slightly non-Gaussian. In the outer region of wall-bound shear flows, $F_u \simeq F_v > 3$ in the outer layer while all other data, i.e. centreline free-shear measurements, indicate that $F_u \simeq F_v < 3$ (not shown). The fact that velocity p.d.f.s are more non-Gaussian than velocity increment p.d.f.s is not surprising. The velocity signal includes all structures at all scales and differencing over large separations is akin to pre-whitening, i.e. a type of smoothing or filtering. Alternatively, the assumption of a slightly non-Gaussian velocity p.d.f. will still result in an approximately Gaussian increment p.d.f., i.e. it would probably be too difficult to detect any non-Gaussianity experimentally. In obtaining (3.1)–(3.11), it was assumed that $\langle\epsilon\rangle = \langle\epsilon\rangle_{iso}$. When $\alpha_{uv} = 1$, (3.1) and (3.2) are identical, as are (3.7) and (3.8), and (3.10) and (3.11); this situation is experimentally rare since global anisotropy exists in nearly every flow. The values of $\langle u^2\rangle^{1/2}$ and $\langle v^2\rangle^{1/2}$ shown in tables 1, 3 and 5 indicate that α_{uv} is consistently smaller

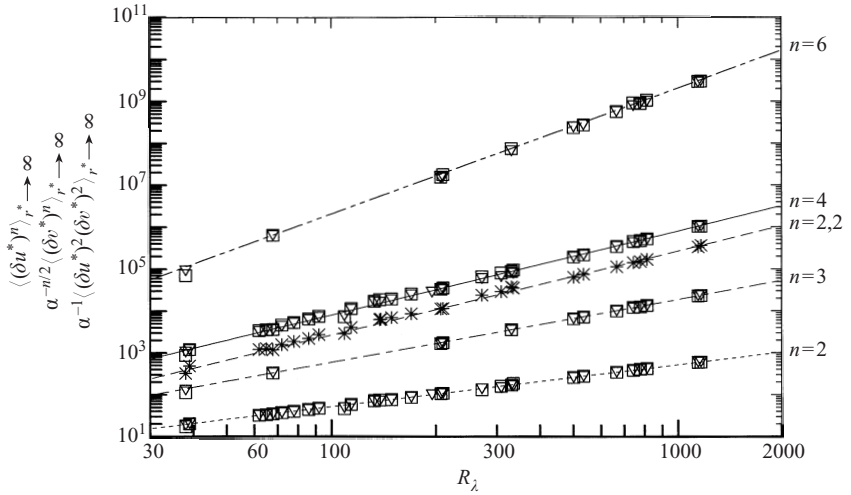

FIGURE 6. R_λ dependence of limiting values, as $r^* \to \infty$, of Kolmogorov-normalized second, third, fourth and sixth-order moments of δu and δv. $\triangledown$, $\langle(\delta u^*)^n\rangle$; $\square$, $\langle(\delta v^*)^n\rangle/\alpha_{uv}^{n/2}$; *, $\langle(\delta u^*)^2(\delta v^*)^2\rangle/\alpha_{uv}$; – – –, equation (3.1); — - —, $(4.51/15^{3/4})R_\lambda^{3/2}$; — —, equation (3.8*b*); ——, equation (3.7); – - - –, equation (3.9).

than 1. For the present turbulent grid flow (table 1), α_{uv} is 0.67 while for the wake (table 1), plane jet (table 5) and circular jet (table 1), it is typically about 0.77. On the axis of the pipe (table 3), α_{uv} averages about 0.69. Recall that (3.3) and (3.4) are identical if $F_u = F_v$ and $\alpha_{uv} = 1$. It is important to note that α_{uv} does enter (3.4) and (3.6) directly and this will be discussed further in § 6. The data in figure 6 are in excellent qualitative agreement with the R_λ^n dependencies indicated by the above equations. In particular, $\langle(\delta u^*)^2\rangle$ is in close agreement with (3.1) while $\langle(\delta v^*)^2\rangle/\alpha_{uv}$ is also consistent with (3.2) and reflects the inequality $\alpha_{uv} < 1$ for large separations. Equations (3.7) and (3.10) also seem to be well satisfied by the measured values of $\langle(\delta u^*)^4\rangle$ and $\langle(\delta u^*)^6\rangle$ for $r^* \gg L^*$. The limiting values of $\langle(\delta v^*)^4\rangle/\alpha_{uv}^2$ and $\langle(\delta v^*)^6\rangle/\alpha_{uv}^3$ again reflect the contribution of the inequality $\alpha_{uv} < 1$. In conclusion, the assumption that both u and v are Gaussian seems reasonable because the resulting assumption that δu and δv are Gaussian when r is large is, experimentally, almost impossible to disprove. In the former case, there is no distinction between contributions to the p.d.f. from different scales whereas in the latter, only the contributions from the largest scales are included.

We next consider the R_λ dependence of the second- and fourth-order moments of δu^* and δv^* in the limit $r^* \to 0$. It is easy to show, assuming isotropy, that (when $r^* \to 0$)

$$r^{*-4}\langle(\delta u^*)^4\rangle \to \left\langle\left(\frac{\partial u^*}{\partial x^*}\right)^4\right\rangle = \frac{1}{15^2}F_{\partial u/\partial x}, \tag{3.12}$$

and

$$r^{*-4}\langle(\delta v^*)^4\rangle \to \left\langle\left(\frac{\partial v^*}{\partial x^*}\right)^4\right\rangle = \frac{4}{15^2}F_{\partial v/\partial x}, \tag{3.13}$$

where $F_{\partial u/\partial x}$ and $F_{\partial v/\partial x}$, are the flatness factors of $\partial u/\partial x$ and $\partial v/\partial x$, respectively. The R_λ dependence of $F_{\partial u/\partial x}$ and $F_{\partial v/\partial x}$ is shown in figure 7; for completeness, results for $F_M \equiv \langle(\partial u^*/\partial x^*)^2(\partial v^*/\partial x^*)^2\rangle/\langle(\partial u^*/\partial x^*)^2\rangle/\langle(\partial v^*/\partial x^*)^2\rangle$, inferred from the limiting values of $r^{*-4}\langle(\delta u^*)^2(\delta v^*)^2\rangle$, have been included. All three quantities appear to

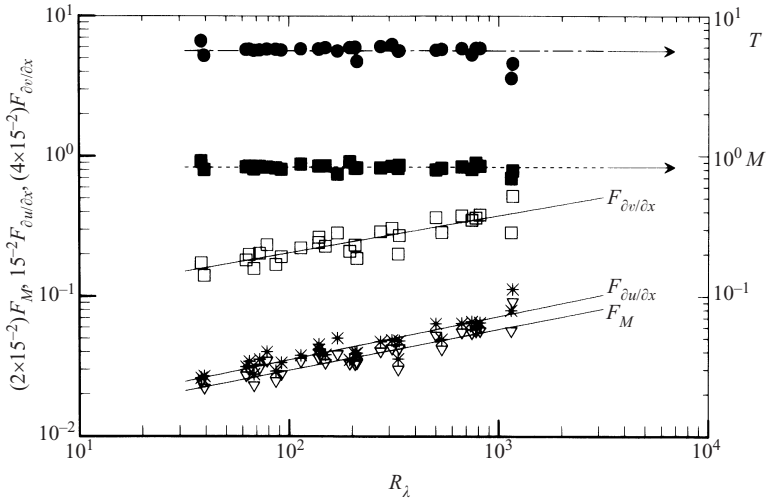

FIGURE 7. R_λ dependence of velocity derivative flatness factors. *, $F_{\partial u/\partial x}$; □, $F_{\partial v/\partial x}$; ▽, F_M; ●, $T \equiv \langle(\partial v^*/\partial x^*)^4\rangle/\langle(\partial u^*/\partial x^*)^4\rangle$; ■, $M \equiv \langle(\partial u/\partial x)^2(\partial v/\partial x)^2\rangle/\langle(\partial u/\partial x)^4\rangle$; —, $R_\lambda^{0.26}$; - - -, $C = 0.84$; — · —, $C = 5.52$.

increase with R_λ at approximately the same rate (the power exponents being 0.26 ± 0.07; 0.26 ± 0.08 and 0.25 ± 0.08, respectively), in particular, there is no indication of a 'transitional' behaviour at $R_\lambda \simeq 700$, as observed by Tabeling *et al.* (1996). Accordingly, the ratios $T \equiv \langle(\partial v/\partial x)^4\rangle/\langle(\partial u/\partial x)^4\rangle$ and $M \equiv \langle(\partial u/\partial x)^2(\partial v/\partial x)^2\rangle/\langle(\partial u/\partial x)^4\rangle$ are, to an excellent approximation, independent of R_λ. This result consolidates the earlier suggestion (Antonia *et al.* 1996), based on a limited R_λ range ($R_\lambda \lesssim 200$), that $F_{\partial v/\partial x}$ increases with R_λ at a rate comparable to that for $F_{\partial u/\partial x}$. The present averaged values of T and M, assuming R_λ independence, are close to 5.52 and 0.84. The power exponents for $F_{\partial u/\partial x}$ and $F_{\partial v/\partial x}$ are in excellent agreement with the model of Pullin & Saffmann (1993; $n = 0.25$) based on the Lundgren–Townsend vortex model for small-scale turbulence. This model predicts that all velocity derivative moments increase at an equal rate. Indeed, Pullin & Saffmann also predict $T = 6$ independently of R_λ, in good agreement with the current experimental results considering the difficulty in acquiring fine-scale measurements.

We finally turn our attention to the R_λ dependence of $\langle(\delta u^*)^2\rangle$, $\langle(\delta v^*)^2\rangle$, $\langle(\delta u^*)^4\rangle$ and $\langle(\delta v^*)^4\rangle$ for a particular value of r. Specifically, we have chosen $r = \lambda$, a separation which nominally falls within or near the beginning of the IR. Figure 8 indicates that these four quantities continue to increase with R_λ, further corroborating the trend of figure 7. As expected, $\langle(\delta u^*)^4\rangle$ and $\langle(\delta v^*)^4\rangle$ increase at a faster rate than $\langle(\delta u^*)^2\rangle$ and $\langle(\delta v^*)^2\rangle$. Their asymptotic rate of increase is larger than that predicted by either the lognormal (Kolmogorov 1962) or β (Frisch, Sulem & Nelkin 1978) models. The latter predictions can be obtained readily from the expression given in Antonia, Satyaprakash & Chambers (1982), i.e.

$$\langle(\delta u^*)^n\rangle \sim R_\lambda^{n/6+\mu_{n/3}},$$

where the exponent $\mu_{n/3}$ depends quadratically on n for the lognormal model

$$\mu_{n/3} = \tfrac{1}{18}\mu n(n-3), \tag{3.14}$$

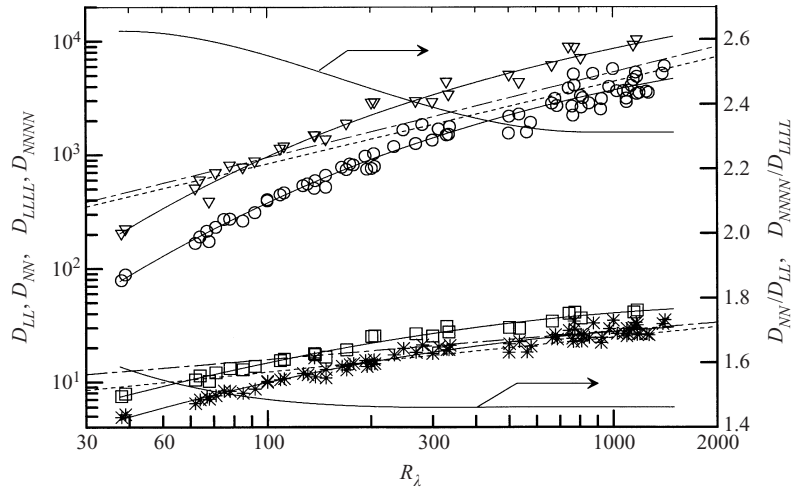

FIGURE 8. R_λ dependence of $\langle(\delta u^*)^2\rangle$, $\langle(\delta v^*)^2\rangle$, $\langle(\delta u^*)^4\rangle$ and $\langle(\delta v^*)^4\rangle$ for $r^* = \lambda^*$. *, $\langle(\delta u^*)^2\rangle$; □, $\langle(\delta v^*)^2\rangle$; ○, $\langle(\delta u^*)^4\rangle$; ▽, $\langle(\delta v^*)^4\rangle$. —, average ratios $\langle(\delta v^*)^2\rangle/\langle(\delta u^*)^2\rangle$ and $\langle(\delta v^*)^4\rangle/\langle(\delta u^*)^4\rangle$; – – –, equation (3.13); — - —, equation (3.14).

and linearly for the β model

$$\mu_{n/3} = \tfrac{1}{3}\mu(n-3). \tag{3.15}$$

The distributions of $\langle(\delta u^*)^n\rangle$ ($r = \lambda$) which correspond to (3.13) and (3.14) for $\mu \simeq 0.25$ (see § 6) are included in figure 8. The difference in the R_λ exponents is not significant between the two models, but it is evident that the measured R_λ dependence is greater than that given by either model and has yet to settle down to a simple power-law. Whereas the LN model underestimates the rate of increase of $\langle(\delta u^*)^4\rangle$ when $r = \lambda$, it appears to overestimate it, albeit slightly, when $r \to 0$. For $\mu = 0.25$, the analysis of Van Atta & Antonia (1980) yields $\langle(\partial u^*/\partial x^*)^4\rangle \sim R_\lambda^{0.42}$, compared with the $R_\lambda^{0.25}$ dependence exhibited in figure 14. The comparison at $r = \lambda$ should be more appropriate than that at $r \to 0$, since $\sigma^2 = A + \mu \ln(L/r)$, where σ^2 is the variance of $\ln \epsilon_r$ (Kolmogorov 1962), cannot be expected to be valid when $r \to 0$.

4. Third-order moments of δu^*

In this section, we examine the R_λ dependence of $\langle(\delta u^*)^3\rangle$ and $\langle|\delta u^*|^3\rangle$. We consider both absolute and non-absolute increments, mainly because $\langle|\delta u^*|^3\rangle$ is used in § 6 to estimate the scaling range exponents via the ESS method. As with the second-order and fourth-order moments (§ 3), we focus on the R_λ dependence of scales in the three different ranges. An overall effect of R_λ on $\langle(\delta u^*)^3\rangle$ and $\langle\ |\delta u^*|^3\rangle$ can be gleaned from figure 9. The overall relative trend between $\langle(\delta u^*)^3\rangle$ and $\langle|\delta u^*|^3\rangle$ is similar in the DR and the IR. The notable difference occurs mainly for large separations ($r \gtrsim L_u$) since non-absolute odd moments should approach zero for sufficiently large separations. In general, the scaling, for both $\langle(\delta u^*)^3\rangle$ and $\langle|\delta u^*|^3\rangle$, is nominally r^{*3} in the DR and r^* for the IR. For $\langle|\delta u^*|^3\rangle$ only, the integral scales behave as $C(R_\lambda)$, where C is a constant which depends on R_λ.

The cornerstone of inertial range theory is the Karman–Howarth–Kolmogorov

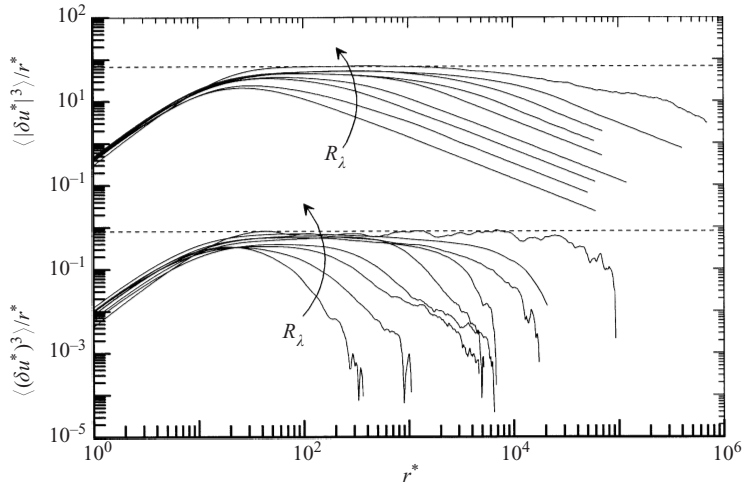

FIGURE 9. A selection of distributions of $r^{*-1}\langle(\delta u^*)^3\rangle$ and $r^{*-1}\langle|\delta u^*|^3\rangle$ with respect to r^*. The r^* behaviours are indicated by dashed lines. The data shown are: GRID, $R_\lambda \sim 68$; pipe, $R_\lambda \sim 112$; pipe, $R_\lambda \sim 171$; RWBL, $R_\lambda \sim 330$; C-J, $R_\lambda \sim 501$; P-J, $R_\lambda \sim 807$; P-J, $R_\lambda \sim 1394$; ASL, $R_\lambda \sim 5680$.

(K–H–K) equation (as referred to by Frisch 1995)

$$\langle(\delta u^*)^3\rangle - 6\frac{\partial\langle(\delta u^*)^2\rangle}{\partial r^*} = -\tfrac{4}{5}r^*. \tag{4.1}$$

When r^* lies in the IR, the second term on the left-hand side is negligible and

$$\langle(\delta u^*)^3\rangle \simeq -\tfrac{4}{5}r^*. \tag{4.2}$$

Evidence of such scaling has been, tentatively, shown for both forced (She *et al.* 1993; Wang *et al.* 1996) and unforced direct numerical simulations (DNS) (Boratav & Pelz 1997) of isotropic box turbulence for relatively low R_λ, although the extent of the linear range was tenuously small. The decaying turbulence simulation of Boratav & Pelz (1997) indicates surprisingly good agreement with (4.2); the corresponding experimental data (Zhou & Antonia 2000) show that, over the IR, the magnitude of $\langle(\delta u^*)^3\rangle$ is smaller than $\frac{4}{5}$, the difference tending to become smaller as R_λ increases (a similar observation is made by Qian (1999) who emphasizes the slow nature of the decay of the finite-Reynolds-number effect). Extrapolation of the data suggests that the difference may disappear for R_λ between 500 and 1000. For the present data, the overall R_λ trend for IR scales is shown in figure 9. Although the extent of the IR is expected to increase with R_λ, this tendency is not apparent in figure 9 either for $\langle(\delta u^*)^3\rangle/r^*$ or $\langle|\delta u^*|^3\rangle/r^*$. There is no strong evidence of either a significant linear region or a region where $-\langle(\delta u^*)^3\rangle/r^*$ is equal to $\frac{4}{5}$. Arguably, the atmospheric data exhibit the most plausible linear region, although the constant is slightly below $\frac{4}{5}$. The 'constant' is plotted in figure 10 both for $\langle(\delta u^*)^3\rangle/r^*$ and $\langle|\delta u^*|^3\rangle/r^*$. The asymptotic 'theoretical' value for $\langle|\delta u^*|^3\rangle/r^*$ is not known. It is evident that both quantities have yet to reach an asymptotic value. In fact, $\langle(\delta u^*)^3\rangle/r^*$ is tending to ~ 0.74 and $\langle|\delta u^*|^3\rangle/r^*$ is approaching ~ 7. Since $\langle\epsilon\rangle_{iso}$ has been used for $\langle\epsilon\rangle$, the actual value of $\langle\epsilon\rangle$ is likely to be larger than $\langle\epsilon\rangle_{iso}$ but not smaller. The shortfall in $-\langle(\delta u^*)^3\rangle/r^*$ cannot therefore be attributed to the unknown true value of $\langle\epsilon\rangle$ – this would only decrease its magnitude.

Another way of examining the R_λ dependence in the IR is to evaluate (4.2) at

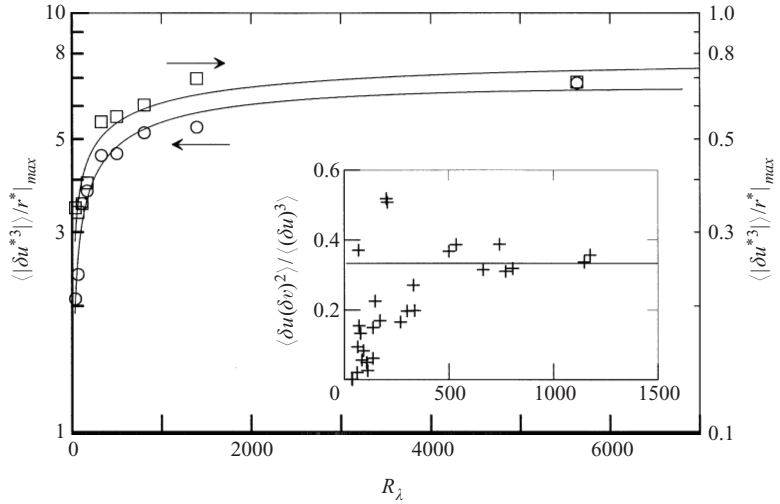

FIGURE 10. Maximum values of $r^{*-1}\langle(\delta u^*)^3\rangle$ and $r^{*-1}\langle|\delta u^*|^3\rangle$. The data correspond to those in figure 9. □, $\langle(\delta u^*)^3\rangle$; ○, $\langle|\delta u^*|^3\rangle$. The inset shows the ratio $\langle\delta u^*(\delta v^*)^2\rangle/\langle(\delta u^*)^3\rangle$ evaluated at $r^* = \lambda^*$ for all X-wire data.

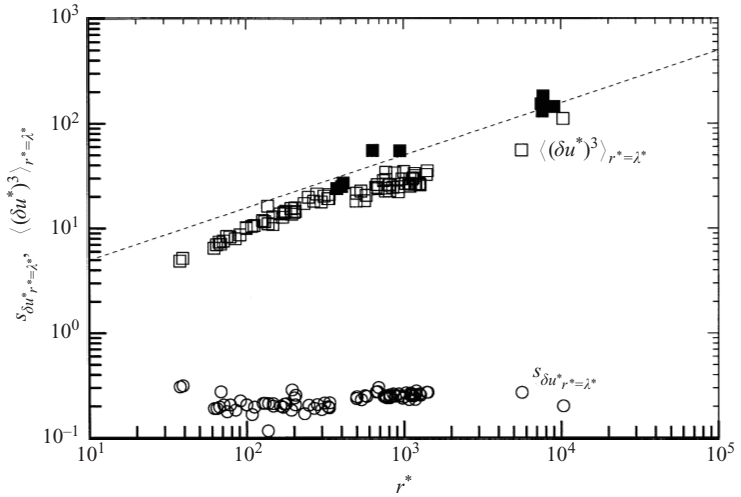

FIGURE 11. R_λ dependence of $\langle(\delta u^*)^3\rangle$, evaluated at $r^* = \lambda^*$ for all data, tables 1–5. Also shown is the corresponding dependence of the skewness $S_{\delta u}$, evaluated at $r^* = \lambda^*$. □, present $\langle(\delta u^*)^3\rangle$; ■, $\langle(\delta u^*)^3\rangle$ taken from Antonia *et al.* (1982); ○, $S_{\delta u} = \langle(\delta u)^3\rangle/\langle(\delta u)^2\rangle^{3/2}$; - - -, $1.574R_\lambda^{1/2}$ (equation (4.3)).

$r = \lambda$. It follows that

$$-\langle(\delta u^*)^3\rangle \simeq \tfrac{4}{5}\lambda^*.$$

For isotropic turbulence, $\lambda^* = 15^{1/4}R_\lambda^{1/2}$ so that

$$-\langle(\delta u^*)^3\rangle = \tfrac{4}{5}15^{1/4}R_\lambda^{1/2} = 1.574R_\lambda^{1/2}. \tag{4.3}$$

This result is shown in figure 11, together with the experimental values of $-\langle(\delta u^*)^3\rangle$ at $r = \lambda$. The latter increase at a rate faster than $R_\lambda^{1/2}$ at least up to $R_\lambda \simeq 10^3$. We have included in this figure the earlier results of Antonia *et al.* (1982); the latter authors concluded, on the basis of relatively few data, that the $R_\lambda^{1/2}$ dependence was satisfied.

A more reasonable conclusion is that (4.3) is likely to be satisfactory only when R_λ exceeds about 10^3. This possibility is of course consistent with the observations made in connection with figure 10 which indicates only an asymptotic approach to (4.2). The skewness $S_{\delta u} \equiv \langle(\delta u)^3\rangle/\langle(\delta u)^2\rangle^{3/2}$ is also shown, for $r = \lambda$, in figure 11. Its magnitude ($\simeq 0.23$) is essentially independent of R_λ. The requirement for a constant of $\frac{4}{5}$ remains a somewhat controversial issue (Monin & Yaglom 1975; Lindborg 1996; Hill 1997). The possibility that both the extent and magnitude of the IR is highly R_λ dependent so that only incomplete similarity is possible while approaching the asymptote (e.g. Barenblatt & Goldenfeld 1995) cannot be dismissed. The other possibility, alluded to in Sreenivasan & Dhruva (1998), is the nature and magnitude of the large-scale, low-wavenumber forcing. In this context, the forced DNS box turbulence results are not so surprising. The unforced, decaying results of Boratav & Pelz (1997) are not so convincing after all. In decaying grid turbulence, there is an additional term in (4.1) (Danaila *et al.* 1999; Lindborg 1999). Danaila *et al.* (1999) showed, for decaying grid turbulence, that the extra term is

$$\frac{\langle U^*\rangle}{r^{*4}}\int_0^{r^*} y^{*4}\frac{\partial}{\partial x^*}\langle(\delta u^*)^2\rangle\,\mathrm{d}y^*. \tag{4.4}$$

This term was shown to be responsible for the non-universal behaviour of the IR. In particular, the measured values of this term accounted quite satisfactorily for the shortfall in the IR 'constant' at least at moderate values of R_λ. Analogously, a term similar to (4.4) satisfactorily accounts for the departure from $\frac{4}{3}$ in Yaglom's equation; the experimental confirmation of this departure was the main focus of the paper by Danaila *et al.* Term (4.4) essentially results from a global non-homogeneity which arises from the lack of homogeneity of the scales of motion at which energy is injected into the flows. For sufficiently large R_λ, order of magnitude arguments (e.g. Lindborg 1996; Antonia *et al.* 1997*b*) suggest that this term should disappear. For non-homogeneous turbulent shear flows, the majority of the flows considered in this paper, the non-homogeneity and anisotropy of the large scales is likely to contribute to the 'shortfall' by leaving its mark on the smaller scales. This influence, of course, should reduce as R_λ increases. More work is needed before the combined effects of R_λ and the mean shear on this shortfall can be quantified adequately. Progress in this direction appears to be under way, e.g. the investigation of Garg & Warhaft (1998) where the shear is kept constant but R_λ is varied.

Figure 6 displays the R_λ dependence of the limiting value of $\langle|\delta u^*|^3\rangle$ as $r^* \to \infty$. The trend is well predicted by assuming that the p.d.f. of $|\delta u^*|$ is Gaussian; the uncertainty in $|\delta u^*|$ and R_λ cannot allow us to distinguish between the Gaussian distribution and any other distribution that deviates only slightly from Gaussianity. In § 3, it was demonstrated that the R_λ dependence of $\langle|\delta u^*|^n\rangle$ and $\langle|\delta v^*|^n\rangle$ for $n = 4$ and 6 can be considered to be Gaussian. For odd moments we must assume that $|\delta u^*|$ is Gaussian. The Gaussian result for the third-order moment is $\langle|\delta u^*|^3\rangle_{r^*\to\infty} = 1.60\langle(\delta u^*)^2\rangle^{3/2}_{r^*\to\infty}$. Using this variance, the R_λ dependence for $\langle|\delta u^*|^3\rangle$ as $r^* \to \infty$ is $\simeq 0.59R_\lambda^{3/2}$. This is indicated in figure 6 and the agreement with experimental data is excellent. Similarly, the result for the limiting value of $\langle|\delta v^*|^3\rangle$ as $r^* \to \infty$ can be estimated as $\simeq 0.59\alpha_{uv}^{3/2}R_\lambda^{3/2}$.

5. Second-order moments of pressure increments

Second-order moments of the pressure increment $\delta p = p(x+r) - p(x)$, where p is the kinematic pressure fluctuation, can be readily inferred from the measured distribution

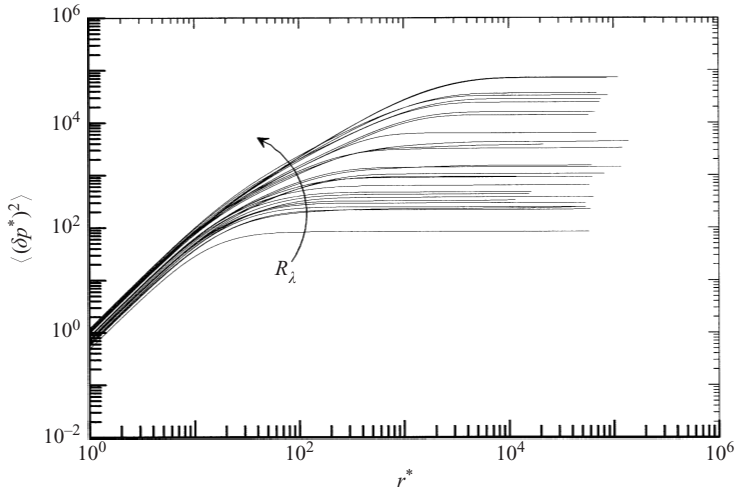

FIGURE 12. Kolmogorov-normalized second-order moment of δp in terms of r^* for $R_\lambda \sim 40 - 1175$. $\langle(\delta p^*)^2\rangle$ is calculated using JGA, equation (5.4). The data correspond to the X-wire data shown in figures 2–7. – – –, $\langle(\delta p^*)^2\rangle \sim r^{*1.2}$.

of $\langle(\delta u)^2\rangle$ provided the joint probability density function of the velocity fluctuations at points x and $x + r$ is assumed to be Gaussian. This is essentially the JGA, as used by several authors, e.g. Batchelor (1951) and Uberoi (1953), which allows quadruple velocity correlations to be expressed in terms of combinations of double velocity correlations, as originally proposed by Millionshchikov (1941).

An expression for the two-point pressure correlation $P(r) = \langle p(x)p(x + r)\rangle$ was given by Batchelor (1951), see also Monin & Yaglom (1975; hereinafter referred to as MY), using JGA

$$P(r) = 2\langle u^2\rangle^2 \int_r^\infty \left(\frac{y - r^2}{y}\right)\left(\frac{\mathrm{d}f}{\mathrm{d}y}\right)^2 \mathrm{d}y, \tag{5.1}$$

where f is the correlation coefficient $\langle u(x)u(x + r)\rangle/\langle u^2\rangle$. A reasonable approximation for locally homogeneous flows is

$$D_{LL} \equiv \langle(\delta u)^2\rangle = 2\langle u^2\rangle(1 - f), \tag{5.2}$$

and

$$\langle(\delta p)^2\rangle = 2\langle p^2\rangle - 2P(r). \tag{5.3}$$

Equation (5.1) can be rewritten as

$$\langle(\delta p)^2\rangle = \int_0^\infty y D'^2_{LL}(y)\,\mathrm{d}y - \int_r^\infty \left(y - \frac{r^2}{y}\right) D^2_{LL}(y)\,\mathrm{d}y, \tag{5.4}$$

where a prime denotes differentiation with respect to y. Equation (5.4) has been used to calculate $\langle(\delta p)^2\rangle$ after least-squares fitting log–log polynomials to the measured distributions of $\langle(\delta u)^2\rangle$ as a function of r. Convergence studies of (5.4) with respect to the upper integration limit required it to be at least $\sim O(10L_u)$. The resulting distributions of $\langle(\delta p^*)^2\rangle$ are shown in figure 12.

At small r^*, the calculated distributions come together but do not collapse. At large r^*, $\langle(\delta p^*)^2\rangle$ approaches a constant value, whose magnitude increases with R_λ. This constant is identifiable with $2\langle p^{*2}\rangle$, as can be inferred from (5.3) when r is sufficiently

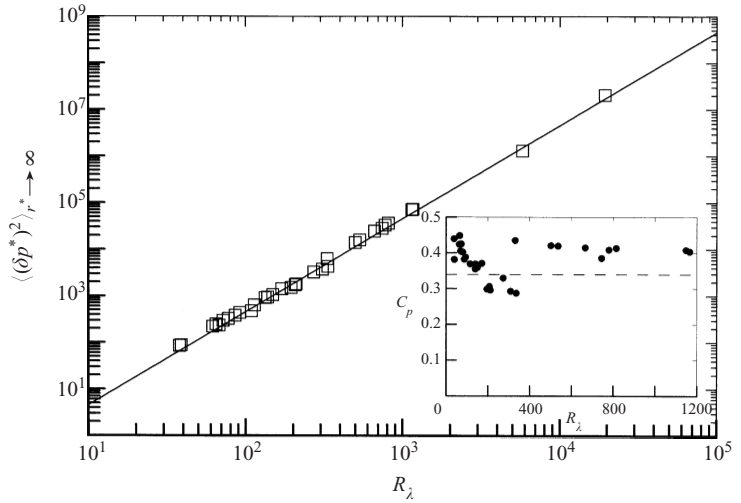

FIGURE 13. R_λ dependence of limiting values of $\langle(\delta p^*)^2\rangle$ calculated using JGA (equation (5.4)) in the limit of $r^* \to \infty$. □, $\langle(\delta p^*)^2\rangle_{r^*\to\infty}$; —, $0.0453R_\lambda^2$. The inset shows the R_λ dependence of the large-scale pressure coefficient, $C_p \equiv \langle p^2\rangle/\langle u^2\rangle^2$. ●, C_p; - - -, $C_p = 0.34$ (Batchelor 1951).

large for $P(r)$ to become negligible. The limiting value

$$\lim_{r^*\to\infty}\langle(\delta p^*)^2\rangle = 2\langle p^{*2}\rangle \tag{5.5}$$

increases in power-law fashion with respect to R_λ. It is of interest to compare this value with previously reported values, based on either measurement or simulation, of the mean-square pressure in different flows. Since the ratio $\langle p^2\rangle/\langle u^2\rangle^2 \equiv C_p$ is usually quoted, it is appropriate to relate $\langle(\delta p^*)^2\rangle$ to this ratio. It was shown, in the context of figure 13, that, for locally isotropic turbulence, $\langle u^{*2}\rangle = R_\lambda/15^{1/2}$. It follows that

$$\lim_{r^*\to\infty}\langle(\delta p^*)^2\rangle = \tfrac{2}{15}C_pR_\lambda^2. \tag{5.6}$$

Batchelor (1951) estimated C_p to be 0.34 for very large Reynolds numbers. Batchelor's calculation used the form of $f(r)$ predicted by Heisenberg (1948). The corresponding form of $D_{LL}(y)$ is

$$D_{LL}(y) = \frac{y^2/15}{(1+30^{-3/2}y^2)^{2/3}}\ . \tag{5.7}$$

Batchelor noted that the accuracy of this estimate depends mainly on the accuracy of $f(r)$. He suggested that $C_p = 0.34$ should be insensitive to the Reynolds number, arguing that, except near $r = 0$, $f(r)$ should be reasonably constant over a wide range of Reynolds number. The estimate of C_p should not be too affected by the joint-Gaussianity assumption since only small scales, which ought to contribute little to $\langle p^{*2}\rangle$, are likely to violate this assumption. There is adequate published evidence (e.g. Schumann & Patterson 1978; MY; Kim & Antonia 1993; Hunt *et al.* 1994) to support JGA at sufficiently large scales.

The dashed line shown in figure 13 corresponds to $C_p = 0.34$; it appears to be in close agreement with the data, over an appreciable R_λ range. This agreement is reasonable since we have verified that (5.7) represents an adequate fit to the measurements at sufficiently large R_λ; we estimate that $D^*_{LL}(u)/r^{*2/3} \sim 2.2$, not 2.0 as predicted by (5.7). The values of C_p are shown in the inset of figure 13 on a linear

scale; a value of about 0.42 seems more appropriate than 0.34. Significant variation has been reported (Hunt *et al.* 1994) for either measured or numerical values of C_p. Measurements in the mixing layer of a relatively high Reynolds number axisymmetric jet indicated a value of 0.42 (George, Beuther & Arndt 1984) while Hinze (1975) reported a value of 0.5. There have been several direct numerical simulations of periodic box turbulence (forced and unforced) with grid resolutions ranging from 32^3 to 512^3 (She *et al.* 1993; Gotoh & Rogallo 1994). A value of about 1 was reported by Schumann & Patterson (1978), Hunt *et al.* (1994) and Pumir (1994). Fung *et al.* (1992) reported values of 0.4 to 0.5 whereas Gotoh & Rogallo (1994, 1999) reported a value of 0.79 for $38 \lesssim R_\lambda \lesssim 172$. Simulations of fully developed channel flow (Kim 1989) indicate a value of about 1.2 ($R_\lambda \simeq 33$, 56) at the centreline. It seems likely, e.g. Gotoh & Nagaya (1999), that the use of the ratio $\langle p^2\rangle/\langle q^2\rangle^2$ instead of C_p would reduce some of the previous discrepancies.

It is of interest to examine how the magnitude of the mean-square pressure gradient $\langle(\partial p/\partial x)^2\rangle$ evolves with R_λ. The evaluation of this quantity has received a fair degree of attention (e.g. Batchelor 1951; Oboukhov & Yaglom 1951; Uberoi 1953; Gotoh & Rogallo 1994, 1999; Gotoh & Nagaya 1999; Vedula & Yeung 1999). Batchelor pointed out that $\langle(\partial p/\partial x)^2\rangle$ is important partly because of its significance in many physical situations and partly because it can be inferred indirectly from observations of the diffusion of marked fluid particles. By analogy to the velocity Taylor microscale λ, Batchelor defined a pressure Taylor microscale

$$\lambda_p^2 = \frac{\langle u^2\rangle^2}{\langle(\partial p/\partial x)^2\rangle}. \tag{5.8}$$

The use of $\langle u^2\rangle^2$ instead of $\langle p^2\rangle$ in the numerator seems justifiable in view of the relative independence of C_p on R_λ (figure 13). Batchelor estimated $\langle(\partial p/\partial x_i)^2\rangle$ using JGA, i.e.

$$\left\langle\left(\frac{\partial p}{\partial x_i}\right)^2\right\rangle = 3\nu^{-1/2}\langle\epsilon\rangle^{3/2}\int_0^\infty y^{-1}[D'_{LL}(y)]^2\,\mathrm{d}y. \tag{5.9}$$

After Kolmogorov-normalizing (5.9) and assuming local isotropy, i.e. $\langle(\partial p/\partial x_i)^2\rangle = 3\langle(\partial p/\partial x)^2\rangle$,

$$\left\langle\left(\frac{\partial p^*}{\partial x^*}\right)^2\right\rangle = \int_0^\infty y^{*-1}[D^{*\prime}_{LL}(y^*)]^2\,\mathrm{d}y^*. \tag{5.10}$$

For the particular form for $D_{LL}(y)$ used by Batchelor, i.e. (5.7)

$$\left\langle\left(\frac{\partial p^*}{\partial x^*}\right)^2\right\rangle \simeq 1.3. \tag{5.11}$$

The present JGA values (figure 14) increase up to $R_\lambda \simeq 300$ and are approximately constant for $R_\lambda \gtrsim 300$. The constant ($\simeq 1.1$) is slightly smaller than that given by (5.11) but nearly the same as that given by Heisenberg (1948). Note that the R_λ increase of $\langle(\partial p^*/\partial x^*)^2\rangle$ in figure 14 simply reflects the increase of $D^{*\prime}_{LL}$ with R_λ. The asymptotic value of $\langle(\partial p^*/\partial x^*)^2\rangle$ can be identified with the constant c_p defined in MY, namely,

$$\langle(\delta p)^2\rangle = c_p\langle\epsilon\rangle^{3/2}\nu^{-1/2}r^2, \tag{5.12}$$

in the limit of small r. Values of c_p obtained via JGA by several authors (e.g. Yaglom 1949; Batchelor 1951) are discussed in MY (p. 409). Yaglom (1949) obtained

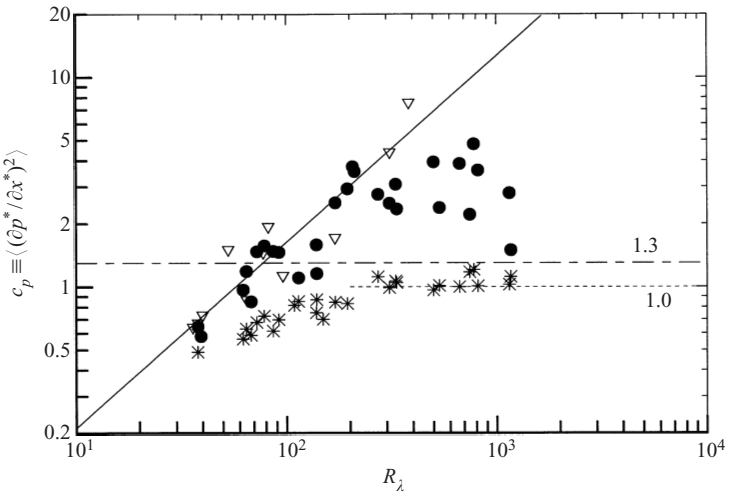

FIGURE 14. R_λ dependence of the small-scale pressure coefficient, $c_p \equiv \langle (\partial p^*/\partial x^*)^2 \rangle$. *, calculated using JGA (equation (5.10)); ●, calculated using HW (equation (5.16)), same X-wire data as used for *; ▽, DNS results, taken from Antonia *et al.* (1998*a*); —, least-squares fit to DNS; — - —, $c_p = 1.3$ (Batchelor 1951); — —, $c_p \simeq 1.0$ (Heisenberg 1948).

$c_p \simeq 0.4/|S_{\delta u}|$ where $S_{\delta u}$, the skewness of δu, was assumed to be constant in the inertial range. This assumption seems adequate allowing for the scatter in the data (e.g. MY). Figure 11 indicates that $S_{\delta u}$ ($r = \lambda$) is approximately independent of R_λ. The average value of $S_{\delta u}$ ($\simeq 0.23$) – this value was also obtained by Garg & Warhaft (1998) in a constant shear flow – implies a value of $c_p \simeq 1.74$, which is significantly larger than the present JGA estimates.

It should be pointed out that the R_λ dependence of the ratio λ_p/λ, as found by Batchelor and MY, is due simply to the R_λ dependence of $\langle u^{*2} \rangle^{1/2}$ since

$$\frac{\lambda_p}{\lambda} = \langle u^{*2} \rangle^{1/2} \frac{\langle (\partial u^*/\partial x^*)^2 \rangle^{1/2}}{\langle (\partial p^*/\partial x^*)^2 \rangle^{1/2}}.$$

For locally isotropic turbulence, $\langle u^{*2} \rangle = 15^{-1/2} R_\lambda$, equation (3.1), and $\langle (\partial u^*/\partial x^*)^2 \rangle^{1/2} = 15^{-1/2}$. It follows that

$$\frac{\lambda_p}{\lambda} = c_p^{-1/2} 15^{-3/4} R_\lambda^{1/2}, \tag{5.13}$$

which is identical to the expression given by Batchelor when $c_p \simeq 1.3$, namely,

$$\frac{\lambda_p}{\lambda} \simeq 0.11 R_\lambda^{1/2} \quad . \tag{5.14}$$

Heisenberg (1948) had obtained a slightly larger value (0.13) for the coefficient, using the spectrum instead of the structure function and assuming statistical independence of Fourier components of the velocity field. Note that 0.13 corresponds to a value of $c_p \simeq 1$, which is in better agreement with our data (figure 15) than $c_p \simeq 1.3$.

Unlike $\langle p^2 \rangle$, $\langle (\partial p/\partial x_i)^2 \rangle$ should receive a significant contribution from small scales. While JGA or Heisenberg's independence hypothesis may be sufficiently accurate for estimating $\langle p^2 \rangle$, it is unlikely to be adequate for calculating $\langle (\partial p/\partial x_i)^2 \rangle$. The accuracy of (5.10) and (5.14) must be questionable in spite of the reasonable support (Batchelor 1951; Uberoi 1953) from turbulent diffusion measurements ($R_\lambda \lesssim 160$) and from the

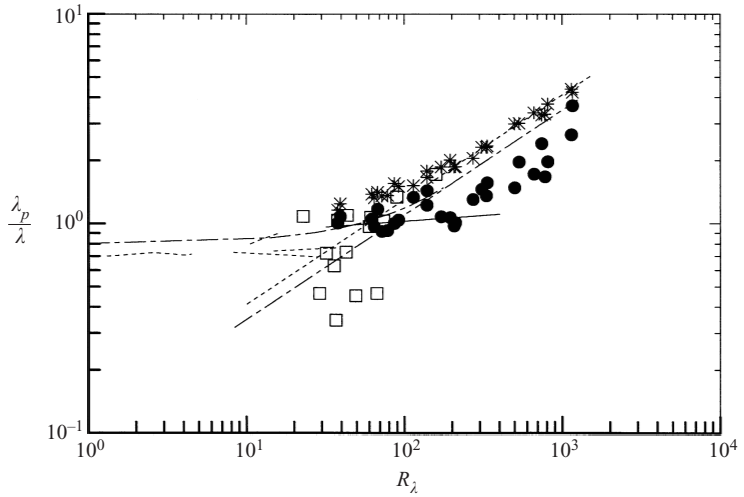

FIGURE 15. R_λ dependence of the ratio of the pressure and velocity Taylor microscales (λ_p/λ). *, calculated using JGA; ●, calculated using HW, same X-wire data as used for *; □, DNS results, taken from Antonia *et al.* (1998*a*); —, least-squares fit to DNS; — - —, equation (5.14) (Batchelor 1951).

small R_λ ($\lesssim 35$) isotropic turbulence simulations of Schumann & Patterson (1978). The latter data, which confirm the theoretical result $\lambda_p/\lambda = 0.707$ ($R_\lambda \to 0$), are included in figure 15.

The previous comments suggest that it is therefore important to avoid JGA when calculating $\langle(\delta p^*)^2\rangle$ at small r^* or evaluating $\langle(\partial p^*/\partial x^*)^2\rangle$. There are two ways of doing this. One is to obtain $\langle(\delta p^*)^2\rangle$ from a direct numerical simulation. The other is to use the relation derived by Hill & Wilczak (1995) which allows $\langle(\delta p)^2\rangle$ to be calculated from a knowledge of $\langle(\delta u)^4\rangle$, $\langle(\delta v)^4\rangle$ and $\langle(\delta u)^2(\delta v)^2\rangle$. Available DNS results for $\langle(\delta p)^2\rangle$ in both homogeneous and non-homogeneous turbulent flows were recently collected by Antonia *et al.* (1999). The range of R_λ extended from 36 to about 380. The results clearly indicated that $\langle(\delta p)^{*2}\rangle$ increased significantly with R_λ at small r^*. The resulting values of $\langle(\partial p^*/\partial x^*)^2\rangle$, which are included in figure 14, are greater and increase ($\sim R_\lambda^{0.9}$) at a faster rate than the present JGA values. Correspondingly, the DNS values of λ_p/λ (figure 15) increase at a much slower rate than the JGA values. The DNS values of $\langle(\delta p^*)^2\rangle$ at $r^* \to \infty$ (not shown here) are of comparable magnitude and increase ($\sim R_\lambda$) at nearly the same rate as the JGA data, thus supporting the earlier claim that JGA appears to be a reliable assumption at sufficiently large values of r.

The relation of Hill & Wilczak (1995),

$$D_p(r) = -\tfrac{1}{3}D_{LLLL}(r) + \tfrac{4}{3}r^2\int_r^\infty y^{-3}[D_{LLLL}(y) + D_{NNNN}(y) - 6D_{LLNN}(y)]\,\mathrm{d}y + \tfrac{4}{3}\int_0^r y^{-1}[D_{NNNN}(y) - 3D_{LLNN}(y)]\,\mathrm{d}y, \qquad (5.15)$$

is based on the assumption of local homogeneity and local isotropy. In (5.15), $D_p(r) \equiv \langle(\delta p)^2\rangle$, $D_{LLLL}(r) \equiv \langle(\delta u)^4\rangle$, $D_{LLNN}(r) \equiv \langle(\delta u)^2(\delta v)^2\rangle$ and $D_{NNNN}(r) \equiv \langle(\delta v)^4\rangle$, the subscript N referring to a direction (y or z) transverse to the flow direction of the mean flow. Distributions of $\langle(\delta p)^2\rangle$ were calculated from (5.15) by Hill & Boratav (1997) (also Boratav & Pelz 1996; Nelkin & Chen 1998) using DNS data for either forced or unforced isotropic turbulence for $R_\lambda \sim 110$–220. These distributions were

found to be in good agreement with the DNS distributions of $\langle(\delta p)^2\rangle$. In contrast, distributions of D_p obtained from (5.15) by using the present measurements of $\langle(\delta u)^4\rangle$, $\langle(\delta v)^4\rangle$ and $\langle(\delta u)^2(\delta v)^2\rangle$ are well behaved only at small r before changing sign. This change occurs when the positive contribution from $\langle(\delta u)^4\rangle$ and $\langle(\delta v)^4\rangle$ is cancelled by the negative contribution from $\langle(\delta u)^2(\delta v)^2\rangle$. This cancellation, which underlines the sensitivity of the calculation, based on (5.15), to the accuracy with which the three fourth-order moments are estimated, was illustrated by Nelkin & Chen (1998) who rewrote (5.15) to make more explicit the relative contributions from these moments. It is unlikely that the cancellation is more critical for measured than numerical data; the application of (5.15) to DNS data for decaying isotropic turbulence (Antonia *et al.* 1998*a*) resulted in a change of sign at quite small values of r^*. The possibility that the change of sign, or cancellation effect, may be caused by a failure of the data to satisfy the local homogeneity requirement of (5.15) cannot be dismissed; this suggestion needs to be investigated further. Alternatively, the definitions of D_{LLNN} and D_{NNNN} given in HW do not have to be restricted to those increments that are experimentally convenient to measure, e.g. a single X-wire probe and Taylor's hypothesis will result in $D_{LLNN}(r) \equiv \langle(\delta u)^2(\delta v)^2\rangle$ and $D_{NNNN}(r) \equiv \langle(\delta v)^4\rangle$. They are not the only L–N pairing possible, yet, as will be shown in § 6, they are the most susceptible to anisotropy.

We limit ourselves here to considering only the behaviour of $\langle(\partial p/\partial x)^2\rangle$, as inferred from (5.15). The resulting relation for $\langle(\partial p/\partial x)^2\rangle$ was given by Hill & Wilczak and is reproduced below in Kolmogorov-normalized form

$$\left\langle\left(\frac{\partial p^*}{\partial x^*}\right)^2\right\rangle = 4\int_0^\infty y^{*-3}[D^*_{LLLL}(y^*) + D^*_{NNNN}(y^*) - 6D^*_{LLNN}(y^*)]\,\mathrm{d}y^*. \tag{5.16}$$

At small R_λ, the resulting values of $\langle(\partial p^*/\partial x^*)^2\rangle$ (figure 14) are comparable in magnitude and rate of growth to the DNS values, thus further raising doubt on the validity of JGA. At the largest R_λ, the values of $\langle(\partial p^*/\partial x^*)^2\rangle$, calculated from (5.16), become constant, as for the JGA values but in contrast to the increasing R_λ trend of the DNS values of $\langle(\partial p^*/\partial x^*)^2\rangle$. We would expect the latter values to be more accurate than either of the former ones since it is consistent with the R_λ increase of all fourth-order velocity derivative moments (figure 7).

6. R_λ dependence of IR scaling exponents

6.1. *ESS scaling exponents*

The scaling exponents of longitudinal increments,

$$\delta S_L(\equiv \delta u_{i,j} = u_i[\tilde{r} + \tilde{x}_0]_j - u_i[\tilde{x}_0]_j,\ i = j),$$

and transverse increments,

$$\delta S_T(\equiv \delta u_{i,j} = u_i[\tilde{r} + \tilde{x}_0]_j - u_i[\tilde{x}_0]_j,\ i \neq j)$$

are discussed in this section (any lack of Kolmogorov normalization should not result in loss of generality). Only for isotropic box DNS simulations of moderate $R_\lambda(\sim 216)$ have the scaling exponents for δS_L [$\langle(\delta S_L)^n\rangle \sim r^{\zeta_L(n)}$; e.g. Cao *et al.* 1996] and δS_T [$\langle(\delta S_T)^n\rangle \sim r^{\zeta_T(n)}$; Chen *et al.* 1997] been, seemingly, directly measured against r. The reason for this success – probably the existence of spatial homogeneity – has been alluded to in § 4. Convincing scale invariance for nth-order moments of δu has yet to be observed in experiments (e.g. Anselmet *et al.* 1984) and therefore we will only

consider relative scaling exponents, estimated using a very general ESS (Benzi *et al.* 1993) formulation, namely,

$$\langle|(\delta\beta_i)^a(\delta\beta_j)^b(\delta\beta_k)^c\ldots(\delta\beta_p)^d|^{n/(a+b+c\ldots+d)}\rangle \sim \langle|(\delta\beta_i)^a(\delta\beta_j)^b(\delta\beta_k)^c\ldots(\delta\beta_p)^d|\rangle^{\zeta(n)}.$$

Here, the ith increment

$$\delta\beta_i(\tilde{r};\tilde{x}_0,t_0) \equiv \beta_i(\tilde{r}+\tilde{x}_0,t_0)-\beta_i(\tilde{x}_0,t), \tag{6.1}$$

can be any variable – e.g. any of the three velocity components or pressure – raised to any order.

In the literature so far there have been several different techniques for measuring δS_T and $\zeta_T(n)$. These depend on whether spatial or temporal increments are measured. In this section, we present results for four relative scaling exponents. The first exponent is the most common longitudinal nth-order scaling exponent $\zeta_L(n)$ (with u and r in the direction of the mean velocity, i.e. $\delta u = u(x+r)-u(x)$ being the more popular) viz.

$$\langle|(\delta S_L)^a|^{n/a}\rangle \sim \langle|(\delta S_L)^3|\rangle^{\zeta_L(n)}.$$

The first transverse exponent to be discussed, $\zeta_{T,1}(n)$ (for the moment we do not distinguish between transverse structure functions which contain transverse velocities and those which include transverse separations; the subscript '1' indicates the first of three types for $\zeta_T(n)$ to be discussed in this section), is relative to δS_L in the region where $\langle(\delta S_L)^3\rangle$ satisfies (4.2) best, namely

$$\langle|(\delta S_T)^a|^{n/a}\rangle \sim \langle|(\delta S_L)^3|\rangle^{\zeta_{T,1}(n)}.$$

Results include those of Antonia & Pearson (1997, 1998); Dhruva *et al.* (1997), Antonia *et al.* (1998*b*), where $\delta S_T \equiv v(x+r)-v(x)$ is achieved with a single-point X-wire type measurement (i.e. temporal increments). A less common definition of transverse scaling exponent is $\zeta_{T,2}(n)$, namely

$$\langle|(\delta S_T)^a|^{n/a}\rangle \sim \langle|(\delta S_T)^3|\rangle^{\zeta_{T,2}(n)},$$

which, while having less theoretical justification than $\zeta_{T,1}(n)$, has been reported with $\delta S_T \equiv u(y+r)-u(y)$ (e.g. Herweijer & Van de Water 1995; Kahalerras *et al.* 1996; Noullez *et al.* 1997) or with $\delta S_T \equiv v(x+r)-v(x)$ (e.g. Camussi *et al.* 1996). Noullez *et al.* (1997) attained their optical measurements using the RELIEF method in the transverse (mean-shear) direction of a circular-jet at moderate R_λ ($\sim$ 810). Kahalerras *et al.* (1996) measured δS_T with a pair of single hot-wire probes with variable transverse separation in a circular jet and in the ONERA S1 wind-tunnel ($R_\lambda \sim 2500$). Herweijer & Van de Water (1995) measured δS_T with a rake of single hot-wire probes separated in the transverse direction on a grid flow at moderate R_λ (230–650) and a circular jet ($R_\lambda \sim 800$). Lastly, a new type of transverse scaling component is investigated, e.g. $\zeta_{T,3}(n)$, namely,

$$\langle|(\delta S_L)^a(\delta S_T)^{2a}|^{n/3a}\rangle \sim \langle|(\delta S_L)^a(\delta S_T)^{2a}|\rangle^{\zeta_{T,3}(n)}.$$

For isotropic turbulence the moment $\langle\delta S_L(\delta S_T)^2\rangle$ should also scale like r (MY; Lindborg 1996). In fact, it is the only third-order moment theory that directly relates δS_T to δS_L.

Figures 16–18 show the R_λ dependence of the four scaling exponents for $n = 2$, 4 and 6, respectively, using the ESS technique. The range used for cross-plotting is centred about the region where $\langle|\delta u^*|^3\rangle/r^*$ is a maximum. Overall, the R_λ dependence

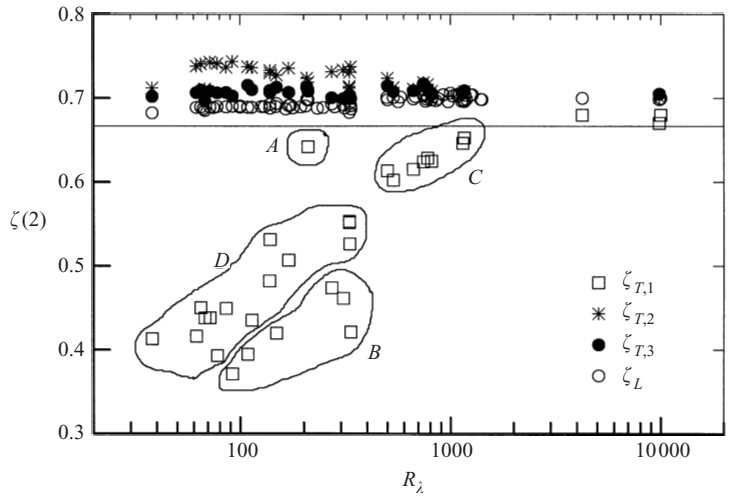

FIGURE 16. R_λ dependence of scaling exponents for $\langle(\delta u)^2\rangle$, $\langle(\delta v)^2\rangle$ and $\langle|\delta u(\delta v)^2|^{2/3}\rangle$ for $R_\lambda \sim 40-10\,000$. In figures 16–18, all data (tables 1–5) are used for $\zeta_L(n)$ and all X-wire data (tables 1, 3 and 5) are used for $\zeta_{T,1}(n)$, $\zeta_{T,2}(n)$ and $\zeta_{T,3}(n)$. Regions marked *A*, *B*, *C* and *D*, as discussed in the text, are shown in figures 16–18. ○, $\zeta_L(2)$; □, $\zeta_{T,1}(2)$; ∗, $\zeta_{T,2}(2)$; ●, $\zeta_{T,3}(2)$. The horizontal line corresponds to $\frac{2}{3}$, the K41 value.

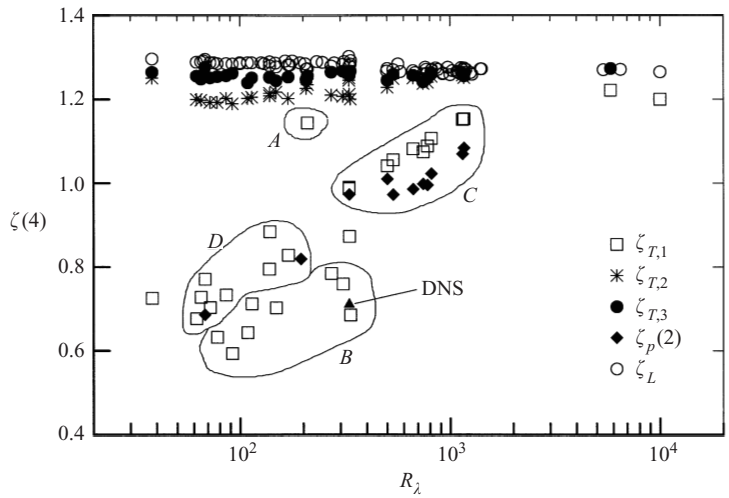

FIGURE 17. R_λ dependence of scaling exponents for $\langle(\delta u)^4\rangle$, $\langle(\delta v)^4\rangle$, $\langle|\delta u(\delta v)^2|^{4/3}\rangle$ and $\langle(\delta p)^2\rangle$. ○, $\zeta_L(4)$; □, $\zeta_{T,1}(4)$; ∗ $\zeta_{T,2}(4)$; ●, $\zeta_{T,3}(4)$; ▽, $\zeta_p(2)$.

is most evident for the highest moment considered, although the following discussion applies equally to $n = 2$ and $n = 4$. ζ_L does show a slight R_λ dependence and this trend is upward increasing for $n = 2$ and downward decreasing for $n = 4$ and $n = 6$ since cross-plotting is relative to $n = 3$ and any trend must change sign as n crosses 3. If a convenient measure for intermittency μ [$\mu \equiv 2 - \zeta_L(6)$] derived from the surrogate of ϵ, is applicable, then figure 18 shows that this relative intermittency factor is increasing with R_λ. This result has been previously reported by Dhruva & Sreenivasan (1998) although their empirical result, included in figure 18, is lower than the present one. Indeed, the asymptotic value is nearly 0.3, which is in close agreement with the observation of Praskovsky & Oncley (1997) for their high R_λ data.

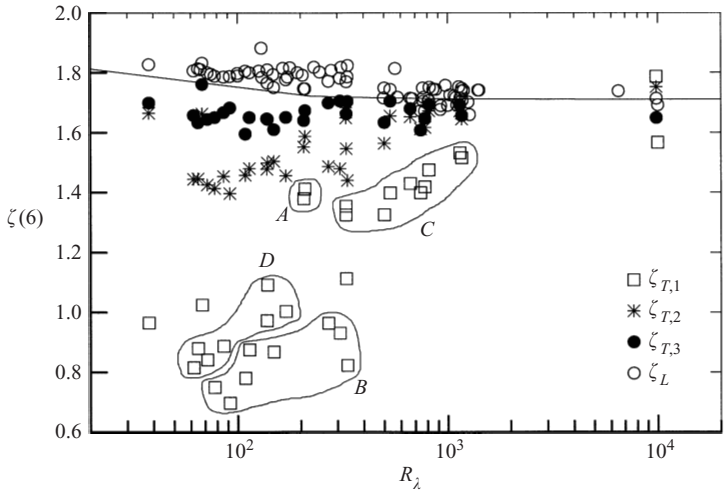

FIGURE 18. R_λ dependence of scaling exponents for $\langle(\delta u)^6\rangle$, $\langle(\delta v)^6\rangle$ and $\langle|\delta u(\delta v)^2|^2\rangle$. ○, $\zeta_L(6)$; □, $\zeta_{T,1}(6)$; *, $\zeta_{T,2}(6)$; ●, $\zeta_{T,3}(6)$. —, Dhruva & Sreenivasan (1998).

The result for $\zeta_{T,1}(n)$ is very R_λ dependent and is consistent with previous observations (e.g. Antonia & Pearson 1997; Dhruva *et al.* 1997; Zhou & Antonia 2000) that the high magnitude of the inequality $\zeta_{T,1}(n) \ll \zeta_L(n)$, at least for small to moderate R_λ, is most probably due to anisotropy. Since $\langle|(\delta v)^a|^{n/a}\rangle$ is cross-plotted against $\langle|(\delta u)^3|\rangle$ – a different variable – there is no change in sign for the R_λ dependence trend from $n < 3$ to $n > 3$ as there is for $\zeta_L(n)$, $\zeta_{T,2}(n)$ and $\zeta_{T,3}(n)$. The existence of the inequality is not too surprising because $\zeta_{T,1}(n)$ is estimated from a cross-plot of two different variables, δu and δv, with different integral lengthscales ($L_u \gg 2L_v$). As α_{uv} becomes smaller than 1, L_v falls below its isotropic value of $\frac{1}{2}L_u$. This reduction results in $\langle|\delta v|^n\rangle$ becoming more quickly decorrelated than $\langle|\delta u|^n\rangle$ – the result is a continual reduction in the local slope as r decreases and an erosion of any IR. However, this effect is reduced, as is the inequality $\zeta_{T,1}(n) \ll \zeta_L(n)$, as R_λ increases and the overwhelming consequences are an increase in the extent of the IR and a reduced influence of large-scale anisotropy as scales reduce in size. Some 'groups' of $\zeta_{T,1}(n)$ results shown in figures 16–18 are worth highlighting. The two high values, marked '*A*' at $R_\lambda \sim 205$, are the results for the high-speed cylinder wake (i.e. $u - v$ and $u - w$ centreline measurements). For these two runs, the 'anisotropy' ratio α_{uv} ($\equiv \langle v^2\rangle/\langle u^2\rangle$) is equal to 0.88 and 0.89, respectively. Conversely, the low group of seven runs marked '*B*' are the off-centreline measurements for the pipe investigation. Within this group, α_{uv} ranged from 0.36 to 0.69 and S^* ranged from 0.06 to 0.077. Although S^* is below the negligible threshold recommended by Kim & Antonia (1993), the increased anisotropy results in a dramatic increase in the inequality $\zeta_{T,1}(n) \ll \zeta_L(n)$. The majority of the data (within areas marked *C* and *D*) appear to follow a plausible R_λ dependence considering that α_{uv} is approximately constant ($0.71 \leqslant \alpha_{uv} \leqslant 0.77$). Although the scarcity of data for $\zeta_{T,1}(n)$ and $\zeta_L(n)$ in the R_λ range 2000–10 000 is regrettable, it is not implausible that the R_λ trend implies a steady reduction in the inequality $\zeta_{T,1}(n) \ll \zeta_L(n)$, which is minimized at $R_\lambda \sim 10\,000$ as suggested by the current atmospheric data.

Before discussing pressure exponents, we note that the R_λ dependence of $\zeta_{T,2}(n)$ is not unlike the results of Herweijer & Van de Water (1995), Camussi *et al.* (1996), Kahalerras *et al.* (1996), Noullez *et al.* (1997). The values of $\zeta_{T,2}(n)$, in our case, are

obtained by cross-plotting against the same component, i.e. $\delta S_T \equiv v(x+r) - v(x)$. Again, a R_λ dependency is evident with a sign change between $n < 3$ and $n > 3$. An inequality between $\zeta_{T,2}(n)$ and $\zeta_L(n)$ exists, but it is smaller than that between $\zeta_{T,1}(n)$ and $\zeta_L(n)$. In fact, when also considering the uncertainty associated with the relatively small sample-size for the higher R_λ runs, it is understandable why some researchers have concluded that $\zeta_{T,2}(n) \simeq \zeta_L(n)$ regardless of whether δS_T is identified with $\langle |u(y+r) - u(y)|^n \rangle$ or $\langle |v(x+r) - v(x)|^n \rangle$, i.e. the cross-plotting of like-variables emphasizes the self-similarity of the nth-moment relative to its third-moment because their origin is the modulus of a common p.d.f. Any connection with turbulence theory is tenuous. Yet, the method has an 'in-built' advantage of minimizing any effects from the mean-shear or the anisotropy. There may be some utility in these exponents in correcting for the effect of S^* or α_{uv}. This possibility appears to be emphasized by the results for $\zeta_{T,3}(n)$, namely, $\langle |(\delta S_L)^a (\delta S_T)^{2a}|^{n/3a} \rangle \sim \langle |\delta S_L (\delta S_T)^2| \rangle^{\zeta_{T,3}(n)}$. In fact, the results appear to be a balance between $\zeta_L(n)$ and $\zeta_{T,2}(n)$ – it is the only exponent that does not show any R_λ dependence in figures 16–18.

Figure 17 contains the results for $\zeta_p(2)$, namely, $\langle (\delta p)^2 \rangle \sim \langle |\delta u_L^3| \rangle^{\zeta_p(2)}$, where $\langle (\delta p)^2 \rangle$ was obtained via JGA, as discussed in § 5. Unlike Boratav & Pelz (1996) and Cao, Chen & Doolen (1999), we find a strong R_λ dependence and the plausible result that $\zeta_p(2)$ asymptotes to a value not too dissimilar to $\zeta_{T,1}(4)$ (which ultimately appears to asymptote to $\zeta_L(4)$) even though, at low R_λ, $\zeta_p(2)$ behaves like $\zeta_{T,1}(2)$. Indeed, the moderate R_λ (~ 380) DNS data of Antonia *et al.* (1999) (though poorly resolved at dissipative scales) also scales like $\zeta_L(2)$ but it is not implausible to assume that it lies within the scatter for $\zeta_p(2)$ in figure 17. Also, the overall trend is in reasonable agreement with the asymptotic result estimated by Nelkin & Chen (1998) from the atmospheric data of Dhruva & Sreenivasan (1998) (i.e. $\zeta_p(2) \sim 1.17$) using the formulation of Hill & Wilczak (1995). All of these results disagree with the assumption that $\zeta_p(2)$ should immediately scale like $[\zeta_L(2)]^2$ i.e. $\zeta_p(2) \simeq 1.4$, but, on the basis of the present JGA results, the IR behaviour of $\langle (\delta p)^2 \rangle$ is considerably more intermittent than $\langle (\delta u)^4 \rangle$ and not entirely unlike $\langle (\delta v)^4 \rangle$.

6.2. *Direct local scaling exponents*

Having considered relative scaling exponents estimated using the ESS technique in § 6.1, it is instructive to consider direct estimates of the local scaling exponents $\zeta_\alpha(n)$. The direct local scaling exponents $\zeta_\alpha(n)$ are here estimated assuming $\langle (\delta \alpha^*)^n \rangle \sim r^{*\zeta_\alpha(n,r^*)}$ ($\alpha = u$ or v), namely

$$\zeta_\alpha(n, r^*) = \mathrm{d}\log[\langle (\delta\alpha^*)^n \rangle]/\mathrm{d}\log[r^*]. \tag{6.2}$$

For the following discussion, the r^* dependence is implied and r^* will be dropped from the notation for $\zeta_\alpha(n)$. By way of an example, figure 19 shows $\zeta_\alpha(n = 4)$ estimated by (6.2) for the Reynolds number range $330 \lesssim R_\lambda \lesssim 1175$. The majority of data shown are plane jet data. A few comments can be made on the general behaviour of $\zeta_u(4)$ and $\zeta_v(4)$. In the DR, $r^* < 10$, $\zeta_\alpha(4)$ is rapidly approaching the viscous requirement of 4 as r^* approaches zero. As r^* increases through the intermediate dissipative range (IDR), considered here to be the interval $10 \lesssim r^* \lesssim 40$, the local values of $\zeta_\alpha(4)$ roll off quickly. For both ranges, i.e. the DR and the IDR, there is reasonable collapse for $\zeta_u(4)$ and $\zeta_v(4)$ – given the difficulty and associated uncertainty in correctly estimating $\langle \epsilon \rangle$. As r^* approaches the IR, there is a considerable reduction in the roll-off rate for both $\zeta_u(4)$ and $\zeta_v(4)$ and the notion of a plateau becomes more plausible – only at high R_λ. After the IR, the roll-off rate for both $\zeta_u(4)$ and $\zeta_v(4)$ then begins to increase again rapidly as r^* approaches L_α^* before eventually

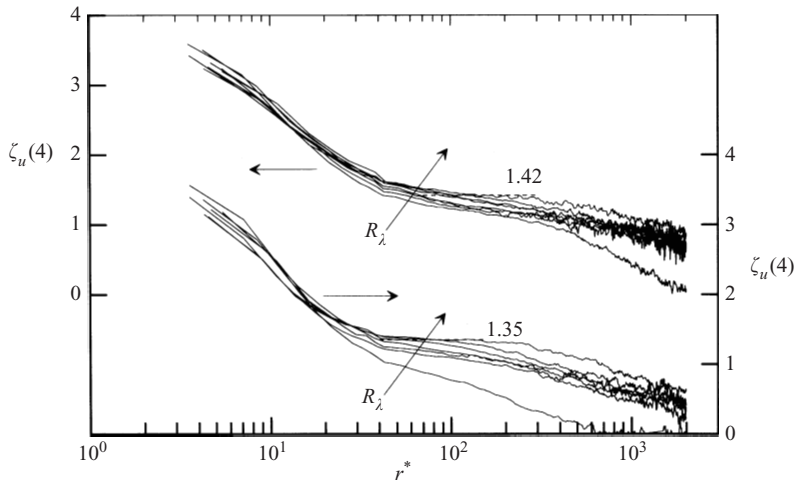

FIGURE 19. R_λ dependence of the direct local scaling exponents $\zeta_\alpha(4, r^*)$ ($\alpha = u, v$) for the rough-wall boundary layer, axi-symmetric jet and plane jet data, $330 \lesssim R_\lambda \lesssim 1175$. The dashed lines are an average over the intervals shown.

disappearing for $r^* \gg L^*_\alpha$ (§ 3). Returning to the region which is assumed to be the IR (§ 4), it is clear that the magnitudes of $\zeta_u(4)$ and $\zeta_v(4)$ increase with R_λ. For the highest R_λ data, there is evidence of a plateau, especially for $\zeta_v(4)$. An average over the intervals $100 \lesssim r^* \lesssim 170$ and $70 \lesssim r^* \lesssim 140$, for $\zeta_u(4)$ and $\zeta_v(4)$, respectively, gives $\zeta_u(4) \approx 1.42$ and $\zeta_v(4) \approx 1.35$. The ratio of these two values is equivalent to that between $\zeta_L(4)$ and $\zeta_{T,1}(4)$ shown in figure 17. A comment is required on the magnitude of $\zeta_u(4)$ and $\zeta_v(4)$ calculated using (6.2). Figure 17 shows that both $\zeta_L(4)$ and $\zeta_{T,1}(4)$, estimated using the ESS technique, are lower than the K41 prediction of $\frac{4}{3}$ and this is commonly thought to be the signature of small-scale intermittency since all similarity hypotheses predict a negative scaling anomaly for $n > 3$. However, the direct local scaling exponents $\zeta_u(4)$ and $\zeta_v(4)$ are both greater than $\frac{4}{3}$ for the highest R_λ plane jet data. We suggest that these higher values reflect the contribution of large-scale anisotropy more than small-scale intermittency. We also note that figures 16–18 indicate that $\zeta_L(n)$ is approximately independent of R_λ, whereas figure 19 shows that $\zeta_u(4)$ continually evolves with R_λ. Such a contradictory result may be construed as an argument against the utility of the ESS technique.

Finally, we will consider direct local scaling exponents $\zeta_u(4)$ and $\zeta_v(4)$ for the highest R_λ data available to us – the ITCE ASL data (table 1) with $R_\lambda \approx 4250$. It is worth recalling that this data is very well resolved in terms of probe resolution ($l^* \approx 2$). Figure 20 shows local values of $\zeta_u(4)$ and $\zeta_v(4)$ calculated by (6.2). The local behaviour of $\zeta_u(4)$ and $\zeta_v(4)$, for the ASL, is similar to that described above for the plane jet data with two notable exceptions. First, the roll-off rate for $\zeta_v(4)$ in the IDR is quicker than that for $\zeta_u(4)$. Secondly, the local values of $\zeta_u(4)$ and $\zeta_v(4)$, within what is assumed to be the IR, are approximately equal with $\zeta_u(4) \simeq \zeta_v(4) \approx 1.37$. These values are based on an average of $\zeta_u(4)$ and $\zeta_v(4)$ over the interval $70 \lesssim r^* \lesssim 140$. The corresponding ESS scaling exponents, $\zeta_L(4)$ and $\zeta_{T,1}(4)$, for the ASL data, shown in figure 17, suggest that there is still approximately 5% disagreement between $\zeta_L(4)$ and $\zeta_{T,1}(4)$. Perhaps this result too can be considered as further evidence questioning the utility of ESS.

A few comments should be made on the actual magnitudes of $\zeta_u(4)$ and $\zeta_v(4)$ for

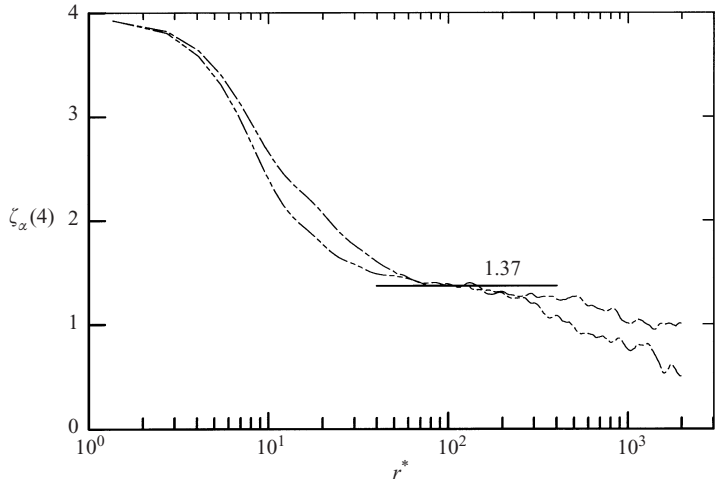

FIGURE 20. R_λ dependence of the direct local scaling exponents $\zeta_\alpha(4, r^*)$ ($\alpha = u, v$) for the atmospheric surface layer data, $R_\lambda \approx 4250$. — - —, $\zeta_u(4, r^*)$; — - - —, $\zeta_v(4, r^*)$; ——, $\zeta_\alpha(4, r^*) \approx 1.37$.

the highest R_λ plane jet results compared to the results for the ASL data. There is no reason to expect the actual magnitudes of $\zeta_u(4)$ and $\zeta_v(4)$ (here we ignore any scaling inequality) from different flows to be equivalent. Indeed, recent theories have been proposed to suggest that large-scale anisotropy, which varies from flow to flow and which is likely to depend on initial/boundary conditions for a particular flow, is a major factor influencing the anomalous contribution to scaling exponents. Preliminary investigations (e.g. Arad *et al.* 1998) have had some success in extracting the anisotropic contribution to the IR scaling. Finally, the approximate equality $\zeta_u(4) \simeq \zeta_v(4)$ suggested by the ASL data further corroborates the conclusion reached from our ESS investigation in § 6.1, namely, when R_λ is large enough to ensure a sufficient separation between energetic and dissipative scales, equality between longitudinal and transverse scaling exponents may be expected. However, the current experimental evidence supports the notion that the magnitude of the IR scaling exponents can be influenced by the degree of large-scale anisotropy.

6.3. *Evidence for the effect of anisotropy on scaling exponents*

In this section, a possible difference between longitudinal and transverse scaling is studied directly by another technique which considers a direct relation between $\langle(\delta u^*)^n\rangle$ and $\langle(\delta v^*)^n\rangle$. We define the relative local scaling exponent, namely,

$$\psi_{uv}(n, r^*) = \mathrm{d}\log\langle[\delta v^*(r^*)]^n\rangle / \mathrm{d}\log\langle[\delta u^*(r^*)]^n\rangle. \tag{6.3}$$

Equation (6.3) resembles the definition of the ESS scaling exponent, (6.1), but now both moments are of order n. If the two structure functions $\langle(\delta v^*)^n\rangle$ and $\langle(\delta u^*)^n\rangle$ scale in a similar manner over the same region of r^*, then $\psi_{uv}(n, r^*) = 1$. Although (6.3) cannot give any information about the actual value of the individual scalings $\zeta_v(n)$ and $\zeta_u(n)$, it can resolve the issue of the inequality between the transverse $\zeta_v(n)$ and longitudinal $\zeta_u(n)$. Figure 21 shows the local relative scaling between $\langle(\delta u^*)^2\rangle$ and $\langle(\delta v^*)^2\rangle$ for the axisymmetric jet, plane jet and atmospheric surface layer data. The greatest departure from 1 of $\psi_{uv}(2, r^*)$ occurs in the region $r^* \approx 10 - 100$ where the DR scales cross over into the IR scales. It is probable that this region reflects the small-scale anisotropy between $\langle(\delta u^*)^2\rangle$ and $\langle(\delta v^*)^2\rangle$. For very small separations

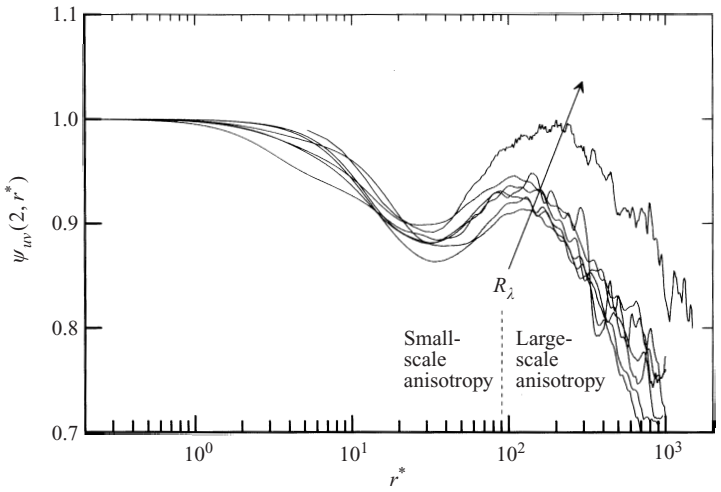

FIGURE 21. R_λ dependence of the relative local scaling exponents $\psi_{uv}(2,r^*)$ for the axi-symmetric jet, plane jet and atmospheric surface layer data, $500 \lesssim R_\lambda \lesssim 4250$.

$r^* \lesssim 5$, all velocity fields are smooth and $\langle(\delta u^*)^2\rangle$ and $\langle(\delta v^*)^2\rangle$ scale in similar manner. Thereafter, the inequality of scaling develops a maximum at approximately the Taylor microscale λ_a^*. Also, figure 21 shows that the maximum value of $\psi_{uv}(2,r^*)$, ignoring the very small separations, occurs in a region beginning at $r^* \approx 150$, and then quickly decays for large-scale separations. Note that the maximum value of $\psi_{uv}(2,r^*)$ is similar to the ratio $\zeta_{T,1}(2)/\zeta_L(2)$ estimated from each of the respective data shown in figure 16. Overall, the behaviour for $\psi_{uv}(2,r^*)$ indicates that both small-scale and large-scale anisotropy inhibits equality of scaling between $\langle(\delta u^*)^n\rangle$ and $\langle(\delta v^*)^n\rangle$. Such a behaviour may be construed as evidence of a lack of separation between the energy and dissipative scales for the current experiments. Although not demonstrated here, the above discussion equally applies to other values of n. It is possible that there is an interesting connection between the local relative scalings $\psi_{uv}(n,r^*)$, relation (6.3), and the velocity variance ratio α_{uv}. We have found that $\psi_{uv}(2,r^*)$ has yet to reach 1.0 in the IR, but the atmospheric data suggests that the possibility of $\psi_{uv}(n,r^*)$ becoming unity in the limit of infinite R_λ cannot be ruled out. The possibility of scaling equality, as R_λ increases, agrees with the conclusions reached for figures 16–18. This leads to the following question: what happens when the transverse increment is composed of the same velocity component as the longitudinal increment? If the transverse direction is chosen to be a homogeneous direction, e.g. the z-direction in the current work, α_{uu} is automatically 1.0 and any influence of large-scale velocity anisotropy is removed from the question of scaling inequality for $\langle(\delta u_L^*)^n\rangle$ and $\langle(\delta u_T^*)^n\rangle$. Such a possibility has been demonstrated in recent experiments in the same plane jet facility (Antonia, Pearson & Zhou 2001) which indicated that the scaling inequality between longitudinal and transverse structure functions is reduced considerably.

Finally, we consider the effect of anisotropy at one value of r, namely $r^* = \lambda^*$; the following discussion relates to figures 8 and 10 which show the R_λ dependence of the ratios $\langle(\delta v^*)^2\rangle/\langle(\delta u^*)^2\rangle$ and $\langle(\delta v^*)^4\rangle/\langle(\delta u^*)^4\rangle$ and $\langle\delta u^*(\delta v^*)^2\rangle/\langle(\delta u^*)^3\rangle$ at $r^* = \lambda^*$, respectively. We have fit and ensemble-averaged two simple power laws to the data using third- and fourth-order log–log polynomials (not shown) and the resulting ratios $\langle(\delta v^*)^2\rangle/\langle(\delta u^*)^2\rangle$, $\langle(\delta v^*)^4\rangle/\langle(\delta u^*)^4\rangle$ in figure 8 and $\langle\delta u^*(\delta v^*)^2\rangle/\langle(\delta u^*)^3\rangle$ in figure 10 are shown as solid lines. The isotropic relationship between $\langle(\delta S_L)^2\rangle$ and $\langle(\delta S_T)^2\rangle$ is

well known:

$$\langle(\delta S_T)^2\rangle = [1 + (r^*/2)\mathrm{d}/\mathrm{d}r^*]\langle(\delta S_L)^2\rangle. \tag{6.4}$$

In the IR, if it is assumed (we ignore any form of intermittency) that $\langle(\delta S_L)^2\rangle \sim C_{11}r^{*\zeta_L(2)}$ and $\langle(\delta S_T)^2\rangle \sim C_{11}r^{*\zeta_L(2)}(1+\zeta_L(2)/2)$ then $\langle(\delta S_T)^2\rangle/\langle(\delta S_L)^2\rangle \sim 1+\zeta_L(2)/2$. For $\zeta_L \sim \frac{2}{3}$, the well-known IR isotropic result $\langle(\delta S_T)^2\rangle/\langle(\delta S_L)^2\rangle = \frac{4}{3}$ follows and it is easily shown that slightly different intermittencies for ζ_L and ζ_T will not drastically change the magnitude of this ratio. Figure 8 shows that $\langle(\delta v^*)^2\rangle/\langle(\delta u^*)^2\rangle$ [$\equiv \langle(\delta S_T)^2\rangle/\langle(\delta S_L)^2\rangle$] asymptotes to ~ 1.44, a value 8.3% greater than $\frac{4}{3}$. The theoretical IR result for $\langle\delta S_L(\delta S_T)^2\rangle/\langle(\delta S_L)^3\rangle$, assuming $\langle(\delta S_L)^3\rangle \sim (\frac{4}{5})r^*$ and $\langle\delta S_L(\delta S_T)^2\rangle \sim (\frac{4}{15})r^*$ is $\frac{1}{3}$. Figure 10 shows that $\langle\delta S_L(\delta S_T)^2\rangle/\langle(\delta S_L)^3\rangle$ asymptotes to a value greater than $\frac{1}{3}$ (~ 0.36). There is no equivalent rigorous theoretical result for $\langle(\delta S_T)^4\rangle$ as a function of $\langle(\delta S_L)^4\rangle$. An empirical relation for fourth-order moments, based on analogies between rigorous second- and third-order theory, has been developed by Ould-Rouis *et al.* (1996). Since no alternative is yet available, we use their relation for $\langle(\delta S_T)^4\rangle$, namely

$$\langle(\delta S_T)^4\rangle = [1 + (9r^*/16)\mathrm{d}/\mathrm{d}r^* + (r^{*2}/16)\mathrm{d}^2/\mathrm{d}r^{*2}]\langle(\delta S_L)^4\rangle. \tag{6.5}$$

If $\langle(\delta S_L)^4\rangle \sim C_{14}r^{*\zeta_L(4)}$ and $\langle(\delta S_T)^4\rangle \sim C_{14}r^{*\zeta_L(4)}(1 + [\zeta_L(4)]/2 + [\zeta_L(4)]^2/16)$ then in the IR, the ratio $\langle(\delta v^*)^4\rangle/\langle(\delta u^*)^4\rangle \sim (1 + [\zeta_L(4)]/2 + [\zeta_L(4)]^2/16)$ is equal to $\frac{16}{9}$ if $\zeta_L(4)$ is $\frac{4}{3}$. Figure 8 shows that $\langle(\delta v^*)^4\rangle/\langle(\delta u^*)^4\rangle$ is about 2.3. As expected, the second-order ratio $\langle(\delta v^*)^2\rangle/\langle(\delta u^*)^2\rangle$ asymptotes more quickly than the fourth-order ratio $\langle(\delta v^*)^4\rangle/\langle(\delta u^*)^4\rangle$. For both these ratios, it would be of interest to calculate the equivalent results for $\delta S_T \equiv u(y+r) - u(y)$. This test would be a useful indicator of the role of global anisotropy, since it is eliminated from relations (6.3) and (6.4).

7. Conclusions

Low-order moments of longitudinal and transverse velocity increments were obtained in many types of turbulent flow, with and without shear and for a relatively wide range of R_λ (40–4250). Some of the data (plane jet, pipe) are new; others have been taken either from the literature, or reduced from earlier measurements in our laboratory. Second-order moments of pressure increments were calculated from the second-order moments of the longitudinal velocity increments with the use of the joint-Gaussian approximation. Each data set was treated in a consistent manner; in particular, attention was paid to the number of independent samples, the extrapolation of the data to Kolmogorov scales and the inclusion of a sufficient number of points to permit the evaluation of power-law exponents in the scaling range.

Several conclusions can be drawn from the Reynolds number behaviour of the increment moments with respect to separations in the dissipative range (DR), the inertial range (IR) and in excess of the integral length scale.

Although the decision to estimate $\langle\epsilon\rangle$ from the isotropic relation $\langle\epsilon\rangle = 15\nu\langle(\partial u/\partial x)^2\rangle$ forces the collapse of $\langle(\delta u^*)^2\rangle$ at small r^*, $\langle(\delta u^*)^2\rangle$ increases with R_λ in the outer part of the DR and throughout the IR. There does appear to be an asymptotic approach to a universal distribution, in the spirit of K41. There is no indication, however, that intermittency disappears, the value of $\zeta_L(2)$ remaining close to 0.70 instead of $\frac{2}{3}$, almost independently of R_λ. The concept of a universal 'Kolmogorov constant' should be tenable if the constant is defined on this basis.

For $\langle(\delta u^*)^2\rangle$, the evolution to an asymptotic state is much faster than for $\langle(\delta v^*)^2\rangle$. This mostly reflects the ever-decreasing effect of anisotropy in the IR. $\zeta_{T,1}(2)$, while always lagging behind $\zeta_L(2)$, approaches the value of $\zeta_L(2)$ only for values of R_λ

exceeding about 10^4. The results for $\zeta_{T,3}(2)$, and to a lesser extent $\zeta_{T,2}(2)$ are much closer to $\zeta_L(2)$ than $\zeta_{T,1}(2)$ since the effect of global anisotropy is removed in the ESS technique. The slight difference between $\zeta_L(2)$ and $\zeta_{T,2}(2)$ or $\zeta_{T,3}(2)$ reflects the skewness of $\delta u(r)$ in the IR.

Both $\langle(\delta u^*)^4\rangle$ and $\langle(\delta v^*)^4\rangle$, as expected for higher-order moments, exhibit a much stronger R_λ dependence than $\langle(\delta u^*)^2\rangle$ or $\langle(\delta v^*)^2\rangle$. In particular, in the limit of small r^*, the magnitudes of $\langle(\partial u^*/\partial x^*)^4\rangle$ and $\langle(\partial v^*/\partial x^*)^4\rangle$ continue to increase with R_λ and do not show the 'transitional' behaviour, around $R_\lambda \simeq 700$, reported by Tabeling *et al.* (1996). The three quantities $F_{\partial u/\partial x}$, $F_{\partial v/\partial x}$ and F_M increase with R_λ at approximately the same rate ($\sim R_\lambda^{0.26}$) and are consistent with the isotropic prediction of Pullin & Saffmann (1993; $\sim R_\lambda^{0.25}$). Also, the ratio of $\langle(\partial v/\partial x)^4\rangle/\langle(\partial u/\partial x)^4\rangle$ (~ 5.52) is close to their prediction (~ 6).

The behaviour of the exponent $\zeta_L(6)$ indicates that, within the framework of RSH, the intermittency parameter 'μ' increases slightly with R_λ, in qualitative agreement with the trend reported by Sreenivasan & Dhruva (1998). In particular, the asymptotic value is nearly 0.3, which is in close agreement with the observation of Praskovsky & Oncley (1997) for their high R_λ data.

Caution is needed in interpreting results for scaling exponents inferred from the ESS method. In particular, the magnitude of scaling exponents which are evaluated directly from the structure functions (e.g. figure 19 when $n = 4$) depends both on r^* and on R_λ over a range which would normally be identified with the IR when ESS is used. The behaviour of directly estimated scaling exponents suggests that the concept of an IR, as proposed in K41, may be approached only asymptotically at very large R_λ.

In the limit $r^* \to \infty$, the power-law exponents of R_λ which describe the rates of increase of the low-order moments of δu^* and δv^* appear to be consistent with the assumed isotropic value of $\langle\epsilon\rangle$. Departures from global isotropy and Gaussianity need to be taken into account when determining the coefficients in the power-law expressions, cf. (3.1)–(3.6).

The validity of the JGA-based calculation of $\langle(\delta p^*)^2\rangle$ improves as r^* increases. In the limit $r^* \to \infty$, the calculated rate of increase of $\langle(\delta p^*)^2\rangle$ or equivalently $\langle p^{*2}\rangle$, is in agreement with Batchelor (1951). The magnitude of $\langle(\partial p^*/\partial x^*)^2\rangle$, calculated using JGA, increases slowly with R_λ and asymptotes to the value estimated by Heisenberg (1948). This variation is, however, unlikely to be correct. DNS results for $\langle(\partial p^*/\partial x^*)^2\rangle$ indicate a much larger rate of increase, more commensurate with that observed for $\langle(\partial u^*/\partial x^*)^4\rangle$ and $\langle(\partial v^*/\partial x^*)^4\rangle$, but are restricted to only relatively small R_λ.

The IR scaling exponents of $\langle(\delta p)^2\rangle$, relative to $\langle|(\delta u)^3|\rangle$, have a significant R_λ dependence. Although $\langle(\delta p)^2\rangle$ has been calculated using JGA we would not expect the real R_λ dependence of $\langle(\delta p)^2\rangle$ to be too dissimilar, although the relative exponents may differ slightly. The exponent $\zeta_p(2)$ behaves very much like $\zeta_{T,1}(4)$ and appears to asymptote to $\zeta_L(4)$, in agreement with the value of $\zeta_p(2)$ calculated by Nelkin & Chen (1998) for the atmospheric data of Dhruva *et al.* (1997), using the formula of Hill & Wilczak (1995).

That there is, for a given R_λ, a whole range of possible values for $\zeta_L(n)$ and $\zeta_T(n)$ is not implausible. For most turbulent flows, local isotropy is the exception rather than the rule, global anisotropy appearing to affect all scales, down to the smallest DR scales in some diminishing degree. It has been shown that an increase in R_λ, for a given flow-type, with α_{uv}, a measure of the global anisotropy, approximately constant, results in a dilation of the IR and improvement in the equality between $\zeta_T(n)$ and $\zeta_L(n)$. Correspondingly, it has also been shown, albeit analogously, that it is naive to

believe that, for anisotropic flows, all measurements of $\zeta_T(n)$, whether by different techniques or definitions, should result in the same value. It is only the increase in R_λ, and the corresponding increase in the separation between λ and L, that appears to rectify this anomaly. Perhaps only a full three-dimensional average of an anisotropic flow would result in a true average value for $\zeta_T(n)$. A scenario of this type could only be expected to be verified computationally.

The support of the Australian Research Council is gratefully acknowledged. R. A. A. is grateful to Dr J. Qian for several helpful comments.

REFERENCES

Anselmet, F., Gagne, Y., Hopfinger, E. J. & Antonia, R. A. 1984 High-order velocity structure functions in turbulent shear flows. *J. Fluid Mech.* **140**, 63–89.

Antonia, R. A., Bisset, D. K., Orlandi, P. & Pearson, B. R. 1999 Reynolds number dependence of the turbulent pressure structure function. *Phys. Fluids* **11**, 241–243.

Antonia, R. A., Orlandi, P. & Pearson, B. R. 1998*a*. Pressure structure functions in isotropic turbulence. In *Proc. 13th Australasian Fluid Mech. Conf.* (ed. M. C. Thompson & K. Hourigan), pp. 607–610. Melbourne.

Antonia, R. A., Ould-Rouis, M., Anselmet, F. & Zhu, Y. 1997*b* Analogy between predictions of Kolmogorov and Yaglom. *J. Fluid Mech.* **332**, 395–409.

Antonia, R. A., Ould-Rouis, M., Zhu, Y. & Anselmet, F. 1997*a* Fourth-order moments of longitudinal and transverse velocity structure functions. *Europhys. Lett.* **37**, 85–90.

Antonia, R. A. & Pearson, B. R. 1997 Scaling exponents for turbulent velocity and temperature increments. *Europhys. Lett.* **40**, 123–128.

Antonia, R. A. & Pearson, B. R. 1998 A comparison between high-order velocity vector and temperature structure functions. *Phys. Rev.* E **57**, 2463–2466.

Antonia, R. A., Pearson, B. R. & Zhou, T. 2000 Reynolds number dependence of second-order velocity structure functions. *Phys. Fluids* **12**, 3000–3006.

Antonia, R. A., Pearson, B. R. & Zhou, T. 2001 Comparison between temporal and spatial transverse velocity increments in a plane jet. *Fluid Dyn. Res.* **28**, 127–138.

Antonia, R. A., Satyaprakash, B. R. & Chambers, A. J. 1982 Reynolds number dependence of velocity structure functions in turbulent shear flows. *Phys. Fluids* **25**, 29–37.

Antonia, R. A., Satyaprakash, B. R. & Hussain, A. K. M. F. 1980 Measurements of dissipation rate and some other characteristics of turbulent plane and circular jets. *Phys. Fluids* **23**, 695–700.

Antonia, R. A. & Smalley, R. J. 2000 Velocity and temperature scaling in a rough wall boundary layer. *Phys. Rev.* E **62**, 640–646.

Antonia, R. A., Zhou, T. & Zhu, Y. 1998*b* Three-component vorticity measurements in a turbulent grid flow. *J. Fluid Mech.* **374**, 29–57.

Antonia, R. A., Zhu, Y. & Shafi, H. S. 1996 Lateral vorticity measurements in a turbulent wake. *J. Fluid Mech.* **323**, 173–200.

Arad, I., Dhruva, B., Kurien, S., L'Vov, V. S., Procaccia, I. & Sreenivasan, K. R. 1998 Extraction of anisotropic contributions in turbulent flows. *Phys. Rev. Lett.* **81**(24), 5330–5333.

Arneodo, A., Baudet, C., Belin, F., Benzi, R. *et al.* 1996 Structure functions in turbulence, in various flow configurations, at Reynolds number between 30 and 5000, using extended self-similarity. *Europhys. Lett.* **34**, 411–416.

Barenblatt, G. I. & Goldenfeld, N. 1995 Does fully developed turbulence exist? Reynolds number independence versus asymptotic covariance. *Phys. Fluids* **7**, 3078–3082.

Batchelor, G. K. 1951 Pressure fluctuations in isotropic turbulence. *Proc. Camb. Phil. Soc.* **47**, 359–374.

Benzi, R., Ciliberto, S., Baudet, C., Ruiz-Chavarria, G. And Tripiccione, R. 1993 Extended self-similarity in the dissipation range of fully developed turbulence. *Europhys. Lett.* **24**, 275–279.

Boratav, O. N. & Pelz, R. B. 1996 Pressure and intermittency in the inertial range of turbulence.

In *Turbulence Modeling and Vortex Dynamics: Proceedings of a workshop held at Instanbul, Turkey* (ed. O. Boratav, A. Eden & A. Erzan), pp. 245–251. Springer.

Boratav, O. N. & Pelz, R. B. 1997 Structures and structure functions in the inertial range of turbulence. *Phys. Fluids* **9**, 1400–1415.

Browne, L. W. B., Antonia, R. A. & Chua, L. P. 1989 Calibration of X-probes for turbulent flow measurements. *Exps. Fluids* **7**, 201–208.

Camussi, R., Barbagallo, D., Guj, G. & Stella, F. 1996 Transverse and longitudinal scaling laws in non-homogeneous low *Re* turbulence. *Phys. Fluids* **8**, 1181–1191.

Camussi, R. & Benzi, R. 1997 Hierarchy of transverse structure functions. *Phys. Fluids* **9**, 257–259.

Cao, N., Chen, S. & Doolen G. D. 1999 Statistics and structures of pressure in isotropic turbulence. *Phys Fluids*. **11**, 2235–2250.

Cao, N., Chen, S. & She, Z.-S. 1996 Scalings and relative scalings in the Navier–Stokes turbulence. *Phys. Rev. Lett*. **76**, 3711–3714.

Chen, S., Sreenivasan, K. R., Nelkin, M. & Cao, N. 1997 A refined similarity hypothesis for transverse structure functions. *Phys. Rev. Lett*. **79**, 2253–2256.

Corrsin, S. 1963 Turbulence: Experimental Methods. In *Handbuch der Physik VIII/2* (ed. S. Flügge & C. Truesdell), pp. 524–590. Springer.

Danaila, L., Anselmet, F., Zhou, T. & Antonia, R. A. 1999 A generalization of Yaglom's equation which accounts for the large-scale forcing in heated grid turbulence. *J. Fluid Mech.* **391**, 359–372.

Dhruva, B. & Sreenivasan, K. R. 1998 On the differences in the scaling of longitudinal and transverse structure functions. Unpublished.

Dhruva, B., Tsuji, Y. & Sreenivasan, K. R. 1997 Transverse structure functions in high-Reynolds number turbulence. *Phys. Rev.* E **56**, R4928–R4930.

Dyer, A. J., Garratt, J. R., Francey, R. J., McIlroy, I. C., Bacon, N. E. *et al.* 1982 An international turbulence comparison experiment (ITCE 1976). *Boundary-Layer Met*. **24**, 181–209.

Frisch, U. 1995 *Turbulence: The Legacy of A. N. Kolmogorov*. Cambridge University Press.

Frisch, U., Sulem, P.-L. & Nelkin, M. 1978 A simple dynamical model of intermittent fully developed turbulence. *J. Fluid Mech.* **87**, 719–736.

Fulachier, L. & Antonia, R. A. 1983 Turbulent Reynolds and Péclet numbers re-defined. *Intl Comm. Heat Mass Transfer* **10**, 435–439.

Fung, J. C. H., Hunt, J. C. R., Malik, N. A. & Perkins, R. J. 1992 Kinematic simulation of homogeneous turbulence by unsteady random Fourier modes. *J. Fluid Mech.* **236**, 281–318.

Garg, S. & Warhaft, Z. 1998 On the small scale structure of simple shear flow. *Phys. Fluids* **10**, 662–673.

George, W. K., Beuther, P. D. & Arndt, R. E. A. 1984 Pressure spectra in turbulent free shear flows. *J. Fluid Mech.* **148**, 155–191.

Gotoh, T. & Nagaya, K. 1999 On universality of statistics of pressure field in homogeneous turbulence. *Extended Abstracts, Proc. IUTAM Symp. on Geometry and Statistics of Turbulence, Hayama, Japan*, pp. 29–30.

Gotoh, T. & Rogallo, R. S. 1994 Statistics of pressure and pressure gradient in homogeneous isotropic turbulence. *Proc. Summer Program*, Center for Turbulence Research, NASA Ames/Stanford University, pp. 189–205.

Gotoh, T. & Rogallo, R. S. 1999 Intermittency and scaling of pressure at small scales in forced isotropic turbulence. *J. Fluid Mech.* **396**, 257–285.

Heisenberg, W. 1948 Zur Statischen Theorie der Turbulenz. *Z. Phys.* **124**, 628–657.

Herweijer, J. A. & Van de Water, W. 1995 Transverse structure functions of turbulence. In *Advances in Turbulence* (ed. R. Benzi), pp. 210–216. Kluwer.

Hill, R. J. 1994 The assumption of joint Gaussian velocities as applied to the pressure structure function. *NOAA Tech. Rep. ERL451-ETL66.*

Hill, R. J. 1997 Applicability of Kolmogorov's and Monin's equations of turbulence. *J. Fluid Mech.* **353**, 67–81.

Hill, R. J. & Boratav, O. N. 1997 Pressure statistics for locally isotropic. *Phys. Rev.* E **56**, R2363–R2366.

Hill, R. J. & Wilczak, J. M. 1995 Pressure structure functions and spectra for locally isotropic turbulence. *J. Fluid Mech.* **296**, 247–269.

Hinze, J. O. 1975 *Turbulence*. McGraw-Hill.

HUNT, J. C. R., MOIN, P., MOSER, R. D. & SPALART, P. R. 1994 Self similarity of two-point correlations in wall bounded turbulent flows. *Proc. Summer Program*, Center for Turbulence Research, pp. 25–36. NASA Ames/Stanford University.

JIMENEZ, J., WRAY, A. A., SAFFMAN, P. G. & ROGALLO, R. S. 1993 The structure of intense vorticity in isotropic turbulence. *J. Fluid Mech.* **255**, 65–90.

KAHALERRAS, H., MALECOT, Y. & GAGNE, Y. 1996 Transverse velocity structure functions in developed turbulence. In *Advances in Turbulence VI* (ed. S. Gavrilakis, L. Machiels & P. A. Monkewitz), pp. 235–238. Kluwer.

KIM, J. 1989 On the structure of pressure fluctuations in simulated turbulent channel flow. *J. Fluid Mech.* **205**, 421–451.

KIM, J. & ANTONIA, R. A. 1993 Isotropy of the small-scales of turbulence at low Reynolds number. *J. Fluid Mech.* **251**, 219–238.

KOLMOGOROV, A. N. 1941 The local structure of turbulence in an incompressible fluid for very large Reynolds numbers. *Dokl. Akad. Nauk. SSSR* **30**, 299–303.

KOLMOGOROV, A. N. 1962 A refinement of previous hypotheses concerning the local structure of turbulence in a viscous incompressible fluid at high Reynolds number. *J. Fluid Mech.* **13**, 82–85.

LINDBORG, E. 1996 A note on Kolmogorov's third order structure-function law, the local isotropy hypothesis and pressure-velocity correlation. *J. Fluid Mech.* **326**, 343–356.

LINDBORG, E. 1999 Correction to the four-fifths law due to variations of the dissipation. *Phys. Fluids* **11**, 510–512.

MILLIONSHCHIKOV, M. D. 1941 Theory of homogeneous isotropic turbulence. *Dokl. Akad. Nauk. SSSR* **32**, 611–614.

MONIN, A. S. & YAGLOM, A. M. 1975 *Statistical Fluid Mechanics.* MIT Press.

NELKIN, M. & CHEN, S. 1998 The scaling of pressure in isotropic turbulence. *Phys. Fluids* **10**, 2119–2121.

NOULLEZ, A., WALLACE, G., LEMPERT, W., MILES, R. B. & FRISCH, U. 1997 Transverse velocity increment in turbulent flow using RELIEF technique. *J. Fluid Mech.* **339**, 287–307.

OBOUKHOV, A. M. & YAGLOM, A. M. 1951 Microstructure of a turbulent flow. *Prokl. Math. Mekh.* **15**, 3–26 (translated as *NACA Rep. TM 1350*, June 1953).

OULD-ROUIS, M., ANTONIA, R. A., ZHU, Y. & ANSELMET, F. 1996 Relations between fourth-order velocity structure functions. *TN FM 96/3*, Department of Mechanical Engineering, University of Newcastle.

PEARSON, B. R. & ANTONIA, R. A. 1997 Velocity structure functions in a turbulent plane jet. *Proc. Eleventh Turbulent Shear Flow Conference*, Grenoble, 3-117–3-121.

PRASKOVSKY, A. & ONCLEY, S. 1997 Comprehensive measurements of the intermittency exponent in high Reynolds number turbulent flows. *Fluid Dyn. Res.* **21**, 331–358.

PULLIN, D. I. & SAFFMANN, P. G. 1993 On the Lundgren–Townsend model of turbulent fine scales. *Phys. Fluids* **5**, 126–145.

PUMIR, A. 1994 A numerical study of pressure fluctuations in three-dimensional, incompressible, homogeneous, isotropic turbulence. *Phys. Fluids* **6**, 2071–2083.

QIAN, J. 1999 Slow decay of the finite Reynolds number effect of turbulence. *Phys. Rev.* E **60**, 3409–3412.

SCHUMANN, U. & PATTERSON, G. S. 1978 Numerical study of pressure and velocity fluctuations in nearly isotropic turbulence. *J. Fluid Mech.* **88**, 685–709.

SHE, Z. S., CHEN, S., DOOLEN, G., KRAICHNAN, R. H. & ORSZAG, S. A. 1993 Reynolds number dependence of isotropic Navier–Stokes turbulence. *Phys. Rev. Lett.* **70**, 3251–3254.

SHE, Z. S. & LEVEQUE, E. 1994 Universal scaling laws in fully developed turbulence. *Phys. Rev. Lett.* **72**, 336–339.

SREENIVASAN, K. R. & ANTONIA, R. A. 1997 The phenomenology of small-scale turbulence. *Ann. Rev. Fluid Mech.* **29**, 435–472.

SREENIVASAN, K. R. & DHRUVA, B. 1998 Is there scaling in high-Reynolds-number turbulence? *Prog. Theoret. Phys. Supp.* **130**, 103–120.

STOLOVITZKY, G., SREENIVASAN, K. R. & JUNEJA, A. 1993 Scaling functions and scaling exponents in turbulence. *Phys. Rev.* E **48**, R3217–R3220.

TABELING, P., ZOCCHI, G., BELIN, F., MAURER, J. & WILLAIME, H. 1996 Probability density functions, skewness, and flatness in large Reynolds number turbulence. *Phys. Rev.* E **53**, 1613–1621.

Tennekes, H. & Lumley, J. L. 1972 *A First Course in Turbulence*. MIT Press.

Uberoi, M. S. 1953 Quadruple velocity correlations and pressure fluctuations in isotropic turbulence. *J. Aero. Sci.* **20**, 197–204.

Van Atta, C. W. & Antonia, R. A. 1980 Reynolds number dependence of skewness and flatness factors of turbulent velocity derivatives. *Phys. Fluids* **23**, 252–257.

Vedula, P. & Yeung, P. K. 1999 Similarity scaling of acceleration and pressure statistics in numerical simulations of isotropic turbulence. *Phys. Fluids* **11**, 1208–1220.

Wang, L.-P., Chen, S., Brasseur, J. G. & Wyngaard, J. C. 1996 Examination of hypotheses in the Kolmogorov refined turbulence theory through high-resolution simulations. Part 1. Velocity field. *J. Fluid Mech.* **309**, 113–156.

Yaglom, A. M. 1949 On the local field of accelerations in turbulent flow. *Dokl. Akad. Nauk. SSSR* **67**, 795–798.

Zhou, T. & Antonia, R. A. 2000 Reynolds number dependence of the small scale structure of grid turbulence. *J. Fluid Mech.* **406**, 81–107.

Zhu, Y., Antonia, R. A. & Hosokawa, I. 1995 Refined similarity hypothesis for turbulent velocity and temperature fields. *Phys. Fluids* **7**, 1637–1678.